# MEASUREMENT OF SEA SCATTER AND BUOY TRACKS AT LONG RANGES BY HIGH-RESOLUTION OTH-B RADAR

Joseph W. Maresca, Jr., et al

Stanford Research Institute

Prepared for:

Office of Naval Research
National Science Foundation

December 1975

*Final Report* *December 1975*

# MEASUREMENT OF SEA SCATTER AND BUOY TRACKS AT LONG RANGES BY HIGH-RESOLUTION OTH-B RADAR

*By:* J. W. MARESCA, JR. J. R. BARNUM

*Prepared for:*

OFFICE OF NAVAL RESEARCH
OCEAN SCIENCE AND TECHNOLOGY DIVISION (CODE 481)
ARLINGTON, VIRGINIA 22217

CONTRACT N00014-74-C-0138 (NR 083-320)



*Sponsored by*

THE OFFICE OF NAVAL RESEARCH
AND THE
NATIONAL SCIENCE FOUNDATION



**STANFORD RESEARCH INSTITUTE**
**Menlo Park, California 94025 · U.S.A.**

SECURITY CLASSIFICATION OF THIS PAGE (When Data Entered)

## REPORT DOCUMENTATION PAGE

READ INSTRUCTIONS BEFORE COMPLETING FORM

1. REPORT NUMBER

2. GOVT ACCESSION NO.

3. RECIPIENT'S CATALOG NUMBER

4. TITLE (and Subtitle)

MEASUREMENT OF SEA SCATTER AND BUOY TRACKS AT LONG RANGES BY HIGH-RESOLUTION OTH-B RADAR

5. TYPE OF REPORT & PERIOD COVERED
Technical Report
1 December 1973 through
31 December 1975

6. PERFORMING ORG. REPORT NUMBER
SRI Project 3071

7. AUTHOR(s)

Joseph W. Maresca, Jr. James R. Barnum

8. CONTRACT OR GRANT NUMBER(s)

N00014-74-C-0138

9. PERFORMING ORGANIZATION NAME AND ADDRESS
Stanford Research Institute
333 Ravenswood Avenue
Menlo Park, California 94025

10. PROGRAM ELEMENT, PROJECT, TASK AREA & WORK UNIT NUMBERS

NR 083-320

11. CONTROLLING OFFICE NAME AND ADDRESS
Office of Naval Research (Code 481)
Arlington, Virginia 22217

12. REPORT DATE
December 1975

13. NO. OF PAGES
~~76~~ 67

14. MONITORING AGENCY NAME & ADDRESS (if diff. from Controlling Office)

15. SECURITY CLASS. (of this report)

UNCLASSIFIED

15a. DECLASSIFICATION/DOWNGRADING SCHEDULE

16. DISTRIBUTION STATEMENT (of this report)

Approved for public release; distribution unlimited.

17. DISTRIBUTION STATEMENT (of the abstract entered in Block 20, if different from report)

18. SUPPLEMENTARY NOTES

Sponsored by the Office of Naval Research and the National Science Foundation.

19. KEY WORDS (Continue on reverse side if necessary and identify by block number)

| | | |
|---|---|---|
| Ocean surveillance | Sea backscatter | Ocean wave spectra |
| Buoy tracking | OTH radar | Ocean currents |
| Ship tracking | HF radar | |
| Wind monitoring | Radar displays | |

20. ABSTRACT (Continue on reverse side if necessary and identify by block number)

This is the final report on a two-year contract entitled "Measurement of Sea Scatter and Buoy Tracks at Long Ranges by High-Resolution OTH-B Radar." The Wide Aperture Research Facility (WARF), a high-resolution skywave high-frequency (HF) radar located in central California, was used to obtain remote measurements of the ocean wave spectrum, overwater wind velocity, and ocean currents in the North Pacific Ocean.

(Abstract Continued)



DD FORM 1 JAN 73 1473

'TION OF 1 NOV 65 IS OBSOLETE

SECURITY CLASSIFICATION OF THIS PAGE (When Data Entered)

19. KEY WORDS (Continued)

20 ABSTRACT (Continued)

The ocean currents were determined by tracking drogued and undrogued drifting buoys carrying a low-power HF repeater. Two drifting buoys, each drogued at 30 m by an 8.5-m parachute, were tracked for one month and four months, respectively, with a position accuracy of 20 km.

Three types of sea backscatter Doppler spectra were recorded to determine the ocean wave spectrum and the wind velocity: (1) backscatter from wide areas of the ocean to develop techniques for mapping wind fields, (2) backscatter from limited areas near research vessels, Navy ships, and ships of opportunity to correlate the observed and radar-measured wind field, (3) long-term coherent samples of backscatter for high-resolution off-line processing to derive the ocean wave spectrum. The results indicate that the mean wind speed can be determined accurately to 2.5 m/s for a range of wind speeds from 5 m/s to 20 m/s, and the mean wind direction can be determined accurately to 16°. A second-order radio wave scattering model developed for HF radar was used to derive the ocean wave spectrum by a trial-and-error calculation. The significant wave height derived from the radar measurements are within 10% of the in situ observation of wave height.

CONTENTS

## ACKNOWLEDGMENTS

We wish to acknowledge the contributions of a number of SRI staff members in this research effort. W. F. Marshall was primarily responsible for data collection. William Preuss, Gary Glassmeyer, and the late Len Schlageter contributed significantly in the operation of the radar system and in data collection. Douglas Westover provided the basic programming for the radar system and reduction of the sea-scatter data. Dorothy McKinney developed the programming for the reduction of buoy and ship positions. Gloria Kojala and Martha Thomson assisted with organizing the data output. Barbara Richards and Jame King typed the manuscripts.

Our colleagues outside SRI during the buoy-tracking effort were Mr. G. McNally at Scripps Institution of Oceanography and Dr. A. D. Kirwan at Texas A&M. The sea-scatter effort was conducted with the cooperation of Dr. R. H. Stewart at Scripps and Dr. A. M. Peterson and his associates at Stanford University.

We are also grateful for the financial support by the Office of Naval Research and National Science Foundation in the NORPAX program.

# I INTRODUCTION

The purpose of the research contract entitled "Measurement of Sea Scatter and Buoy Tracks at Long Ranges by High-Resolution OTH-B Radar" is to determine the feasibility of using a skywave HF radar to remotely measure the ocean wave spectrum, the oceanic wind field, and the ocean currents in the North Pacific Ocean. The work was performed over a two-year period extending from 1 December 1973 through 31 December 1975. Our work involved the cooperation, support, and coordination of the scientists at Scripps Institution of Oceanography (SIO); Stanford University (SU); and Texas A & M University (TAMU).

This report consists of a brief outline of our work (Sections II through IV), and copies of papers submitted or accepted for publication (Appendices A, B, and C).

## II MEASUREMENT OF SEA-SCATTER AND BUOY TRACKS BY HIGH-RESOLUTION OTH-B RADAR

SRI's participation during the first year of the NORPAX effort was coordinated with and in support of the more basic oceanographic research by the scientists at SIO, SU, and TAMU. This effort was divided into two tasks. The first task was the recording and spectral analysis of sea backscatter data over predesignated areas in the North Pacific Ocean. Doppler spectra were given to the scientists at SIO for analysis of wind velocity. The second task was the recording and analysis of backscatter range-azimuth tracking data to determine the position of a network of drifting buoys, each instrumented with an HF repeater.

### A. Tracking Drifters

The tracking of drifting buoys was begun during the NORPAX Pole Experiment and was successfully completed with an rms position error of 20 km. Six drifting buoys, three drogued at 30 m with 8.5-m-diameter parachutes and three undrogued, were launched January 29, 1974. Two of the drifters (one drogued and one undrogued) malfunctioned immediately; two of the drifters (both undrogued) failed early in the experiment or rapidly drifted out of the radar coverage; one drifter (drogued) was tracked for one month, after which it failed; and one drifter (drogued) was tracked for four months. The results of this effort are found in a report by Marshall and Barnum.[1]* The tracking information was given

*References are listed at the end of the main text. References for the appendices are listed at the end of each appendix.

to the scientists at SIO and TAMU for interpretation. The results and interpretation of the long-term trajectories are presented by Kirwan and McNally.[2]

B. Sea Backscatter Data

Recording and processing of the backscatter measurements were also begun during the NORPAX Pole Experiment. The results of this effort are also found in Marshall and Barnum.[1] Both wide-area scans in the vicinity R.V. Flip and longer dwells over specific areas of the North Pacific were made. The wide-area scans were processed for 12.8 s of coherent integration time for 21 range lines (1.5 km per range line), and the longer dwells were processed for 25.6 and 51.2 s of coherent integration time over 8 range lines. The longer dwells were taken each day between 2300 and 2400 GMT when the HF repeater aboard R.V. Flip was turned on. The longer-dwell sea backscatter data taken at this time were not analyzed because of multipath. Better spectra could have been obtained by operating at a different time of day. For the wide-area scans taken during the Pole Experiment and during a March 1974 storm passage west of 150° W, the sea backscatter Doppler spectra were obtained for analysis and correlation with the observed wind speed and direction obtained from R.V. Flip and other ship reports. These data were given to the scientists at SIO for analysis and comparison with the ground truth. The results of the correlations between wind speed and direction have been presented by Stewart and Barnum.[3]

## III REMOTE SENSING OF SEA SURFACE MOVEMENT AT LONG RANGES BY IONOSPHERICALLY PROPAGATED BACKSCATTER WITH HIGH RESOLUTION

The second year in the NORPAX effort was a coordinated undertaking between the scientists at SIO and SU. The purpose of this research was to record, spectral-analyze, and correlate the backscatter measurements with observed values of surface winds and surface waves obtained from ships of opportunity. As part of this effort, basic questions about the optimal spectral processing necessary to interpret the sea backscatter data were investigated.

The results are presented in three papers (Refs. 4-6). Wind speed estimates were improved by normalizing the data by the inverse of the square root of the frequency. Accuracies of 2.5 m/s were obtained. The results of the wind-speed correlation, the applicability of the technique, and a discussion of the potential errors are discussed by Maresca and Barnum[4] in a paper accepted for publication in 1977, further extending the discussion in Ref. 3.

The ability to map the entire wind direction field is discussed by Barnum, Maresca, and Serebreny[5] in a paper accepted for publication in 1977. This paper is included in our final report as it is directly pertinent to NORPAX work even though the sea backscatter data were taken prior to our contract. The high-resolution measurements in the vicinity and across the atmospheric front are especially noteworthy.

Ionospherically clean Doppler spectra were obtained for coherent integration times of 102 s. Johnstone's[7] second-order radio-wave scattering model for bistatic radars was used in a trial-and-error calculation to determine the ocean wave spectrum and is discussed by

Maresca, Johnstone, and Barnum[6] in a paper to be submitted to the Journal of Geophysical Research. Ocean wave spectra were not available for comparison, but hourly observation of the wave height by two Navy ships in the area agreed within 10% of the significant wave height calculated from the radar-derived wave spectra.

## IV PRINCIPAL RESULTS

High-frequency skywave radar radio wave measurements of wave height and wind speed are consistent with theory.

The ability to scan large areas allows the derivation of the entire wave and wind field for large storm passages. The high resolution of WARF allows investigation of intense gradients across low-pressure cells and across atmospheric fronts.

Wind speed estimates were accurate to 2.5 m/s and wind direction estimates were accurate to 16°. Wave height measurements derived from the radar-measured ocean wave spectrum were accurate to within 10% of the observed wave heights. Skywave radar position fixes used to measure ocean currents by tracking drifting buoys were accurate to within 20 km.

The ionosphere will support propagation sufficiently to make the same type of measurements as line-of-sight radar with approximately the same accuracies. The important difference is the occasional degradation of skywave data by unstable propagation.

For a limited data set, it was found that the incoherent averaging of 4 to 8 Doppler spectra obtained at the same range line or the incoherent averaging of 1 to 2 Doppler spectra obtained over an 8-range-line average will produce a stable mean; the ratio of the Bragg lines was used as a parameter. Increasing the coherent integration time did not significantly affect the mean but did allow for greater resolution in the Doppler spectra.

## REFERENCES


1. W. F. Marshall and J. R. Barnum, "Measurement of Sea Scatter and Buoy Tracks at Long Ranges by High-Resolution OTH-B Radar," Technical Report 1, Contract N00014-14-74-C-0138 (NR 083-320), Stanford Research Institute, Menlo Park, Calif. (May 1975).

2. A. D. Kirwan, Jr., and G. McNally, "A Note on Observations of Long Term Trajectories of the North Pacific Current," J. Phys. Oceanog., Vol. 5, No. 1, pp. 188-191 (January 1975).

3. R. H. Stewart and J. R. Barnum, "Radio Measurements of Oceanic Winds at Long Ranges: An Evaluation," Radio Science, Vol. 10, No. 10, pp. 853-857 (October 1975).

4. J. W. Maresca, Jr., and J. R. Barnum, "Measurement of Oceanic Wind Speed from HF Sea Scatter by Skywave Radar," accepted by IEEE Trans. on Antennas and Propagation, Vol. AP-25, No. 1 (January 1977).

5. J. R. Barnum, J. W. Maresca, Jr., S. M. Serebreny, "High-Resolution Mapping of Oceanic Wind Fields with Skywave Radar," accepted by IEEE Trans. on Antennas and Propagation, Vol. AP-25, No. 1 (January 1977).

6. J. W. Maresca, Jr., D. L. Johnstone, and J. R. Barnum, "Measurement of the Ocean Wave Spectrum by HF Skywave Radar," to be submitted to J. of Geophys. Res.

7. D. L. Johnstone, "Second-Order Electromagnetic and Hydromagnetic Effects in High-Frequency Radio-Wave Scattering from the Sea," Technical Report No. 3615-3 (SEL-75-004) (Ph.D. Dissertation), Contracts N00014-75-C-0356 and N00014-69-A-0200-6012, Stanford Electronics Laboratories, Stanford, Calif. (March 1975).

Appendix A

# HIGH-RESOLUTION MAPPING OF OCEANIC WIND FIELDS WITH SKYWAVE RADAR

by

James R. Barnum, Member IEEE
Joseph W. Maresca, Jr.
Sidney M. Serebreny

Accepted for Publication in
IEEE Transactions on Antennas and Propagation
(Special Issue on Radio Oceanography)

September 1975

This work was performed by Stanford Research Institute, Menlo Park, California, and was sponsored in part by the Office of Naval Research and the National Science Foundation as part of the North Pacific Experiment (NORPAX).

Appendix A

# HIGH-RESOLUTION MAPPING OF OCEANIC WIND FIELDS WITH SKYWAVE RADAR


## ABSTRACT

The direction of the mean surface wind field in the North Pacific Ocean was mapped on 25 and 26 September 1973 over an area of $3 \times 10^6$ $(km)^2$ by OTH-B HF radar. A spatial resolution of 60 km in range and 15 km in cross range were used at points spaced by 150 km in range and 80 km in cross range. Wind directions were inferred from the upwind/downwind first-order Bragg ratio and the measure of the maximum ratio occurring for radial winds at points near each observation. Detailed measurements of the wind speed and direction were used to define the position of an atmospheric cold front. Range resolutions of 3 km are achieved with the WARF radar and are essential to the analysis of atmospheric fronts and the gradient of the wind stress across intense cyclones.


## I INTRODUCTION

Measurements of ocean surface winds are important to the understanding of air/sea interaction. Along with desert and polar areas, the oceans comprise vast data-sparse regions. The violent and destructive tropical cyclones are spawned and grow to great dimensions and intensities in such areas. On these occasions, ocean surface measurements are especially desirable.

Inferences of ocean surface waves and winds have been achieved remotely with the use of high-frequency (HF) radar [1]-[8]. Radar echoes from the sea at decameter wavelengths are caused by Bragg resonance of the radio waves with individual ocean waves and groups

of interacting waves [3],[6]. First-order Bragg resonance with ocean waves of one half the radio wavelength produce the strongest scatter. With skywave [2] (ionospheric) propagation at 6 to 30 MHz those waves have 4.0-to-1.8-s periods, respectively, and are tightly coupled to the local winds especially for frequencies above 10 MHz. Higher-order scatter is produced by ocean waves of all lengths greater than half the radio wavelength, and the most significant returns are found at Doppler frequencies near the first-order Bragg return [5].

Long and Trizna [1] were first to publish radar maps of ocean wind direction obtained at long ranges with skywave propagation [2]. Barrick et al. [3] inferred significant wave height from surface wave radar echoes at close ranges. Ahearn et al. [4] mapped ocean wind directions with the method in [1], and also attempted to infer ocean wind speeds from the ocean scatter magnitude near zero Doppler. Tyler et al. [5] inferred the directional spectrum of sea waves near Wake Island with a bistatic surface-wave radar. Johnstone [6] published a detailed treatment of the first- and second-order theory of HF scatter from the sea, and found agreement in the measure of wind speed with surface-wave sea-scatter recordings near Wake Island during the same experiment [5].

A new method for inferring wind fields at long ranges by skywave radar was presented by Stewart and Barnum [7]. Wind direction was inferred from the first-order Bragg scatter ratio from approaching and receding waves, using a new model for the ocean wave directional spectrum that is a function both of wind speed and radio frequency. The wind speed was inferred from the Doppler spectrum width centered on the strongest Bragg return at a level 10 dB lower than the Bragg peak. Maresca and Barnum [8] have improved this measure of wind speed by accounting for the effect of radar frequency and have discussed the theoretical limitations. Reliable measures of ocean surface winds

accompanied the data discussed in [7] and [8], from which we now deduce accuracies of ±16° in wind direction and ±2.4 m/s in wind speed within one standard deviation relative to the measures in situ.

Skywave radar coverage far exceeds that of HF surface wave. HF radar analysis of large weather disturbances such as storm systems would be possible only with the larger coverage. By comparison, the use of surface-wave radar has contributed most extensively to our understanding of the complete Doppler frequency spectrum of sea scatter [3],[5],[6]. Since the lower atmosphere has negligible effect on the coherence of the propagating wave, and only a single mode (the surface wave) is present, very long coherent data integrations are thereby permitted (e.g., tens of minutes). Hence, the Doppler resolution can be extremely high. Such integration followed by several incoherent spectrum averages yields a smooth estimate of the mean spectrum amplitudes of the scatter. Essentially, two potential problems exist with the use of ionospheric propagation for the purpose of sea scatter analysis: (1) a coherence time limit caused presumably by the motion of fine-scale irregularities; and (2) the simultaneous reception of more than two propagating modes (multipath) from different areas of the sea. The coherence time allowed by the ionosphere will generally limit the Doppler resolution to between 0.1 and 0.01 Hz [8],[9] at middle latitudes, and can be expected to be poorer at more northerly latitudes [9]. The highest coherence is found for E-layer reflection, because it affords the least penetration of the ionosphere. Unfortunately, this low layer prohibits propagation beyond about 2000 km range via a single hop, and it is generally absent between sunset and sunrise. Multipath propagation is evident in a large percentage of data recorded [8] and is considerably more prevalent at ranges exceeding 3000 km via single-hop F-layer propagation [7]. Multipath will always obscure some portion of the sea scatter Doppler spectrum, when viewed as a whole, but will not necessarily limit inference of

wind direction or speed from the scatter located near the two first-order Bragg returns [8].

This paper illustrates the results of a two-day skywave radar scatter experiment over the Pacific Ocean. The direction of the ocean wind field was mapped to high resolution over $3 \times 10^6$ km$^2$ and the wind velocity was detailed across a cold front. It will be shown that significant changes in wind direction occur over space scales on the order of 20 km or less, such that high radar resolution was indispensible. Ionospheric effects on these data are discussed.

## II THEORY

The method for determination of wind speed from the second-order-scatter contribution to the Doppler spectra has been discussed elsewhere [7],[8].

The determination of wind direction for the September 1973 experiment is analogous to that of Long and Trizna [1]. To infer the wind direction we assumed that the 2-to-3-second waves responded within a short time (approximately one hour) to the local winds, and that the measure really represents the mean wind over the same period of time.

The sea-wave energy directional spectrum, $F(\theta)$, for $|\theta| \leq \pi/2$ was assumed to be somewhere between semi-isotropic and cosine squared:

$$F(\theta) = A + B \cos^2 \theta \qquad (1)$$

where A and B are arbitrary constants, and $\theta$ is the angle between the wind and wave directions. It was also found empirically [1] that

$$F(\pi - \theta) = \frac{F^2(\pi/2)}{F(\theta)} \quad . \qquad (2)$$

We define the ratio of first-order Bragg line amplitudes in the approaching and receding directions by $X(\theta)$, where

$$X(\theta) \triangleq \frac{F(\theta)}{F(\pi - \theta)} \quad . \tag{3}$$

Nearest each data scan we measure the maximum $X(\theta)$ at $\theta = 0$ or the inverse of the minimum X at $\theta = \pi$, with either one called $X_m$, and we define $X(\pi/2) = 1$. We then find that

$$X(\theta) = \begin{cases} [1 + K \cos^2 \theta]^2 \ldots & 0 \leq |\theta| \leq \pi/2 \\ [1 + K \cos^2 \theta]^{-2} \ldots & \pi/2 \leq |\theta| \leq \pi \end{cases} \tag{4}$$

where $$K = \sqrt{X_m - 1} \quad . \tag{5}$$

Equation (4) can be inverted to express $\theta$ as a function of $X(\theta)$.

In [1] and [4] we find that $X_m$ was assumed to be constant for all data recorded, regardless of the operating frequency or wind speed. In light of the work by Tyler et al. [5] we cannot hold $X_m$ constant for our experiment. By assuming constant $X_m$ we fix the sea wave directional spectrum for all time. Tyler et al. concluded that $F(\theta)$ is a function of both the ratio frequency and wind speed, and use a different functional representation for $F(\theta)$, which is a modification of the form suggested by Longuet-Higgins, Cartwright, and Smith [10]. When we constrain the $F(\theta)$ in [5] to match observed values of $X_m$ and $X(\pi/2) = 1$, we calculate a maximum of only 11° difference between $\theta$ predicted, using $F(\theta)$, by both methods. We have used the measured $X_m$ nearest to each recorded spectra, thereby updating Eq. (4) with Eq. (5) for all data reported herein. $X_m$ varied between 14 and 24 dB, with a mean of 21 dB. We believe that any effects on $F(\theta)$ caused by changes in radio frequency and wind speed have thus been partially accounted for.

## III RADAR CHARACTERISTICS

The Wide Aperture Research Facility (WARF) was designed originally for high-resolution DOD-related applications, and has not been described to any great detail in the open literature. The reader is referred to a paper by Skolnik and Headrick [11] for an introduction to OTH radar practices, and to a paper by Croft [2] for illustrations of data recorded via skywave propagation. Some details regarding the WARF radar, and examples of swept-frequency ocean backscatter amplitude were published by Barnum [12]. A more recent summary was published in report form by Marshall and Barnum [13]. The WARF coverage is shown in Fig. 1.

Briefly, WARF is a bistatic system with 185 km separation between transmitter and receiver in central California. Four megawatts of average effective radiated power (ERP) are directed toward the scattering area. This large-receiving-aperture (2.55 km) radar yields a radar antenna beamwidth of 1/3° at 20 MHz. A time-delay resolution of 20 $\mu$s was used to record our data (where 1 $\mu$s is close to 150 m of ground range for this skywave experiment). Thus, we processed ocean areas with dimensions of 15 km (average) in cross range and 3 km in range. A total of 21 range lines were averaged incoherently to smooth the scattering statistics, resulting in a net spatial average of 15 km × 60 km.

Performance assurance of the WARF backscatter system is achieved through simultaneous operation of two additional systems. The first system provides continuous surveillance of the HF operating frequencies available for propagation to ensure that interfering signals that can confuse the spectral information in the backscatter are not present in the swept bandwidth. The second system is a low-power wide-frequency swept-backscatter system used to estimate the mode of signal propagation to the area of interest and to specify usable operating frequencies. Examples of such data were published by Croft [2] and Barnum [12].

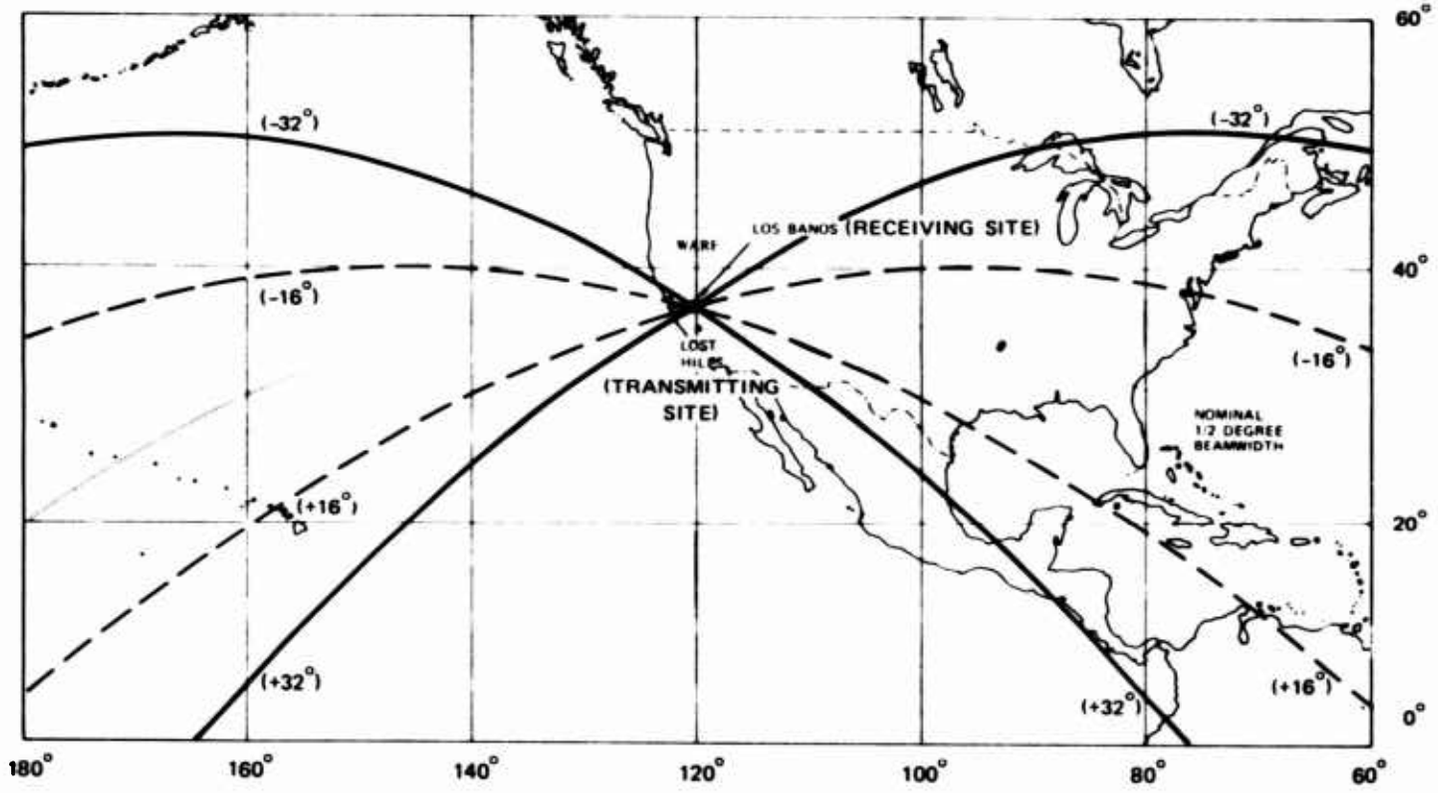


FIGURE 1 WARF RADAR AZIMUTH COVERAGE TO THE EAST AND WEST OF CALIFORNIA

## IV SPECTRAL PROCESSING

Figure 2 illustrates the basic form of data output from the radar processor. Three-dimensional displays of backscatter amplitude versus time delay (range) and Doppler frequency are first processed by means of a double Fourier transform of the deramped SFCW signals. The Doppler coverage extends from +2.5 Hz to -2.5 Hz for an SFCW repetition rate of 5 Hz. The raw samples are weighted by a cosine-squared window to reduce frequency sidelobes. A coherent integration of 12.8 s was used exclusively with the data discussed in this paper.

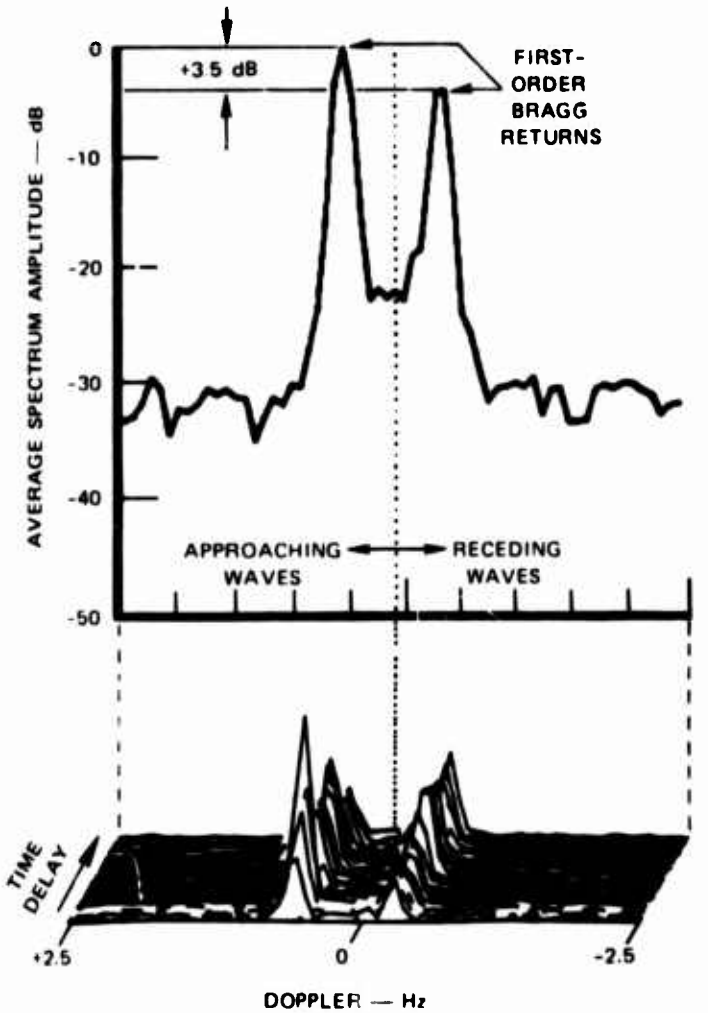


FIGURE 2 EXAMPLE OF THE OCEAN-WAVE BACKSCATTER DOPPLER SPECTRA. Bottom is spectrum vs range (time delay) at a single azimuth. Top is the average of all range lines.

Incoherent spectrum averaging is used to smooth the statistical variation of sea scatter amplitude. This variation was found to resemble a Gaussian process both in time and space. Two incoherent time averages and 21 spatial (range-cell) averages were performed prior to each spectrum output in this experiment and should produce a very smooth estimate of the representative scatter spectrum [8].

Figure 3 illustrates the portion of the real-time processor output used in this experiment. These data were updated once per minute. Three adjacent antenna beams, spaced by one-half degree, were sampled and processed simultaneously. A log of radar operating parameters was recorded automatically. The Bragg line ratio X, and spectrum width B

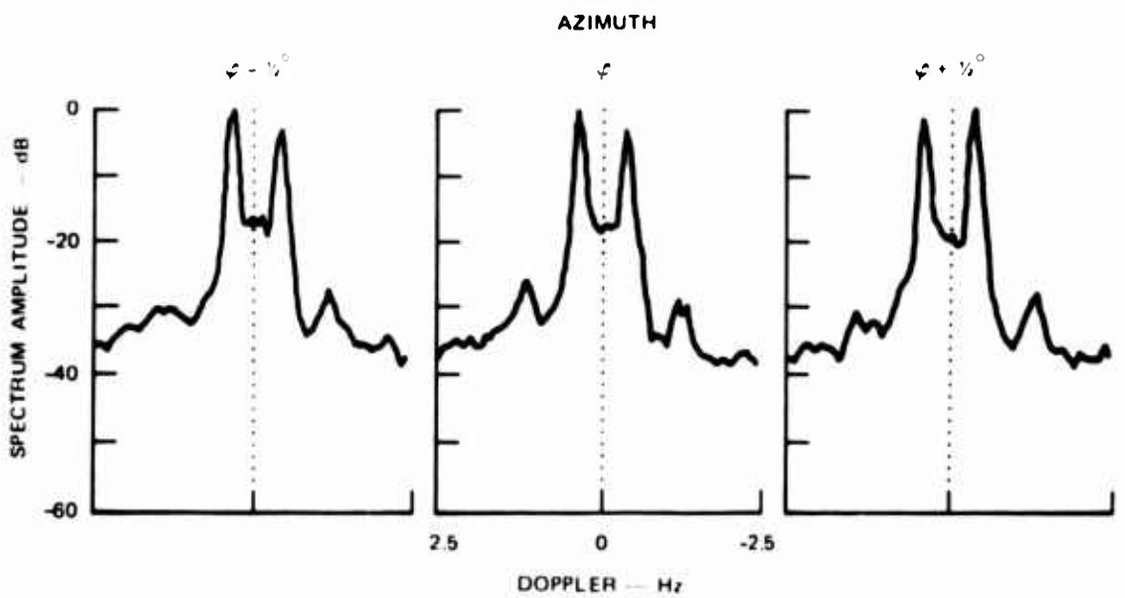


26 SEPTEMBER 1973
1630 GMT
19 ms

| Az | X (dB) | B+ | B- |
|---|---|---|---|
| φ - ½° | 1.2 | 0.299 | 0.303 |
| φ | 3.8 | 0.251 | 0.270 |
| φ + ½° | -2.4 | 0.274 | 0.263 |

FIGURE 3 EXAMPLE OF THE REAL-TIME BACKSCATTER DISPLAY USED FOR RECORDING DATA FOR WIND-FIELD MAPPING. Each such display is updated once per minute at a new ocean location. The center azimuth was used to map wind fields.

were also calculated automatically for each azimuth, and are labeled X and B, respectively, on Fig. 3.

## V DATA COLLECTION AND INTERPRETATION

Data similar to Fig. 3 were recorded sequentially by stepping every 2° in azimuth at a constant radar time delay and frequency. The frequency was changed prior to each scan to ensure adequate propagation along each scan. Time delays were stepped in 1-ms increments between 10 and 27 ms on the first day and between 13 and 25 ms on the second day using F2-layer propagation. The longer ranges were sampled earlier in the day because multipath was least prevalent at those times.

Propagation conditions were usually different at the two ends of an azimuth sector, such that more optimum time delays and/or frequencies could have been chosen for different portions of each scan. Ionospheric multipath often appeared over portions of a scan at azimuths where the skip distance was approached too closely. The calculation of $X(\theta)$ for wind direction was rarely affected by multipath, but not all spectra can be reduced for wind speed using B. The data beyond 20 ms (2000 km) were the most often perturbed.

Figure 4 illustrates spectra from a portion of one such azimuth scan on 26 September 1973. These data illustrate three results from this experiment: the occasional observation of multipath, as shown at -6° azimuth (276° True from the radar); a double wind shift, noted by reversals in the sign of X across a weather front; and a more gradual wind direction change SW of a high pressure area. Multipath occurs on other spectra to a lesser degree (e.g., at -4°) but did not degrade the calculation of B.

All spectra from the experiment were first reduced for the Bragg line ratio, X, and this was plotted vs. azimuth, parametric in time delay. Figure 5 is an example of some of these plots on 26 September

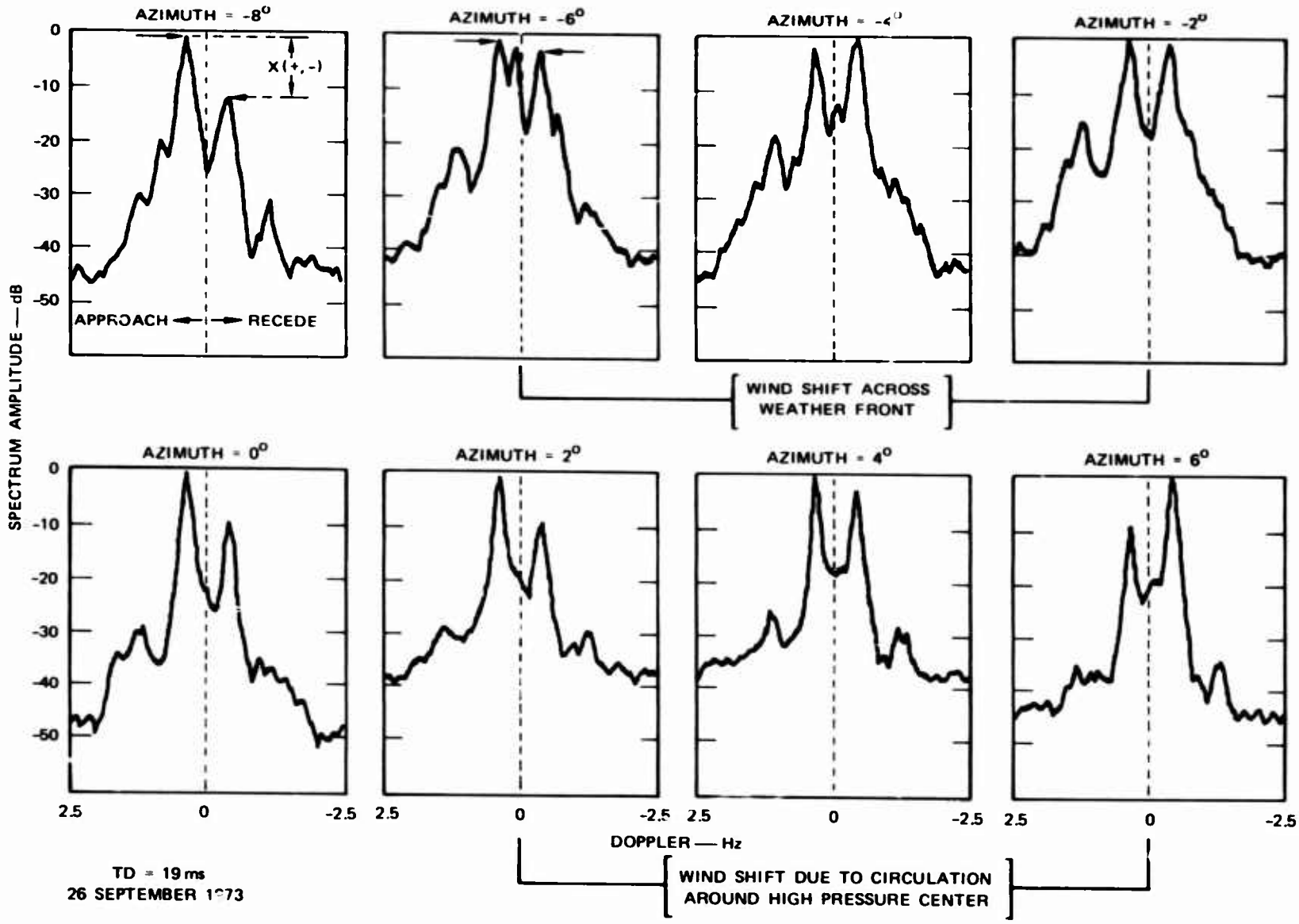


FIGURE 4 EXAMPLES OF SPECTRA FROM ONE OF THE AZIMUTH SCANS AT 19 ms ON 26 SEPTEMBER 1973. Illustrates the effects on X caused by (a) cold-front crossing at -6° to -2°; (b) circulation around a high at 2° to 6°.

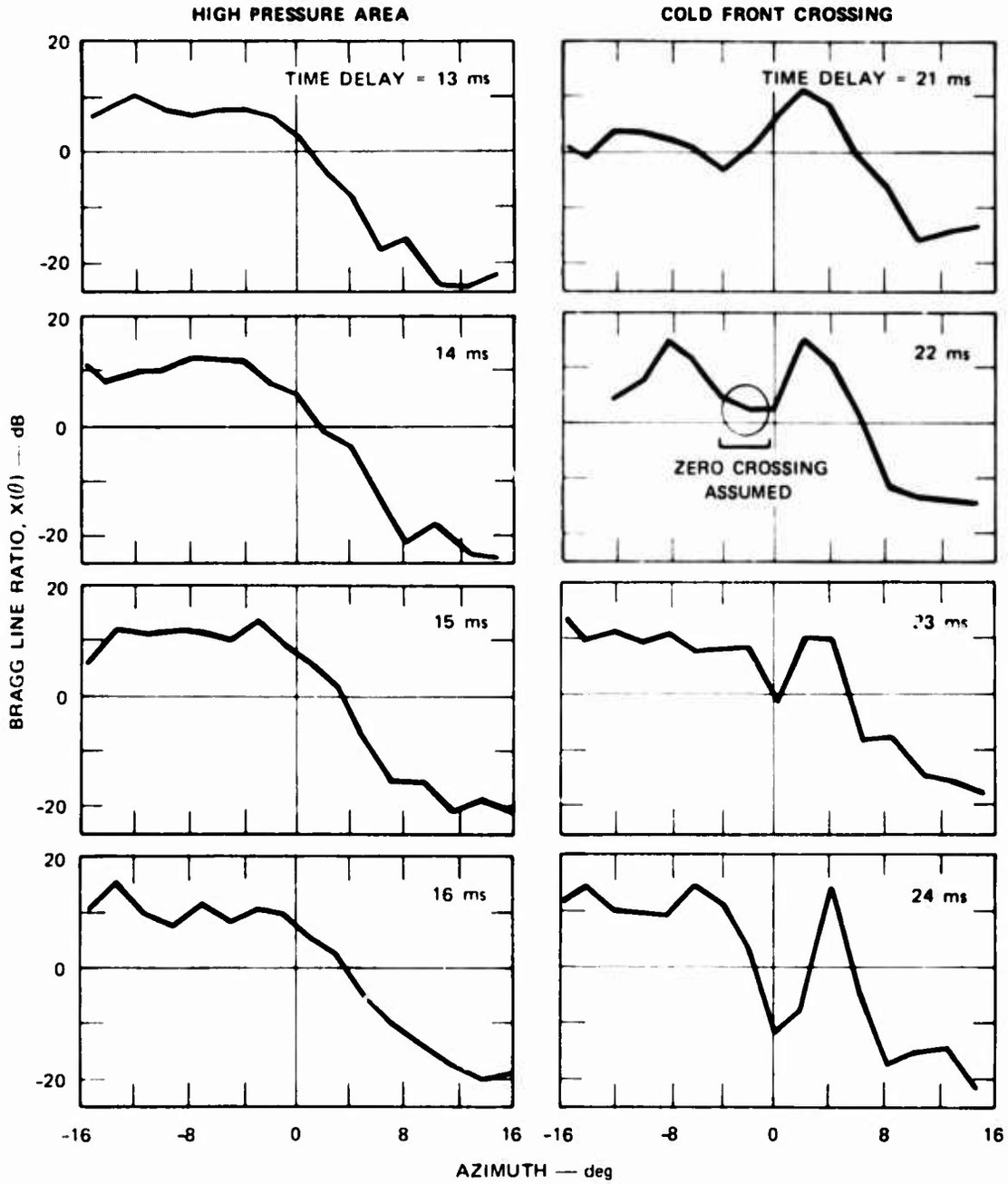


FIGURE 5 BRAGG-LINE RATIO, X(θ) vs RADAR AZIMUTH AT EIGHT TIME DELAYS ON 26 SEPTEMBER 1973. Circulation to the SW of a high-pressure system was sampled by the data between 13 and 16 ms, while a cold front was crossed by the scans between 21 and 24 ms.

1973. The plots on the left of the figure represent scans to the west of an anticyclone and to the east of a cold front. The maximum observed values of X (in absolute dB) occurred in the trade wind region, since the winds were approximately parallel to the radar heading. The plots on the right side of the figure contain radar crossings of a weather front that noticeably interrupted the otherwise continuous nature of X versus azimuth. The weather front usually caused a double zero crossing in X that is seen at azimuths between -6° and 2° in Fig. 5, depending on the time delay. These zero crossings essentially accounted for net changes in wind direction exceeding 180°. Note that the minimum in X between these crossings advances in azimuth from -4° at 21 ms delay, to between 0° and 2° at 24 ms delay. This trend was interrupted by a dip at -2° at 22 ms with a lack of a zero crossing. Since crossings were also observed at 19 ms and 20 ms delays, a reversal of wind direction was therefore assumed to occur at -2° azimuth at 22 ms.

The left/right ambiguity in $\theta$ [1],[4] was resolved by general knowledge of the overall circulation around the high-pressure cell shown on the NWS map and cloud photograph. Each zero crossing yields a wind that is crosswise to the radar bearing, a condition that usually occurred across the cold front.

## VI RADAR WIND FIELD MAPS

The radar-derived wind field for the first day, 25 September 1973, is shown in Fig. 6, and is compared with the relevant portion of the National Weather Service (NWS) surface analysis for 1800 GMT. As indicated on the table in Fig. 6, the radar data were recorded between the hours of 1855 GMT and 2512 (0112) GMT. We expect the data at the lower time delays (later in the day) to disagree with the ship reports taken some 6 to 7 hours earlier.

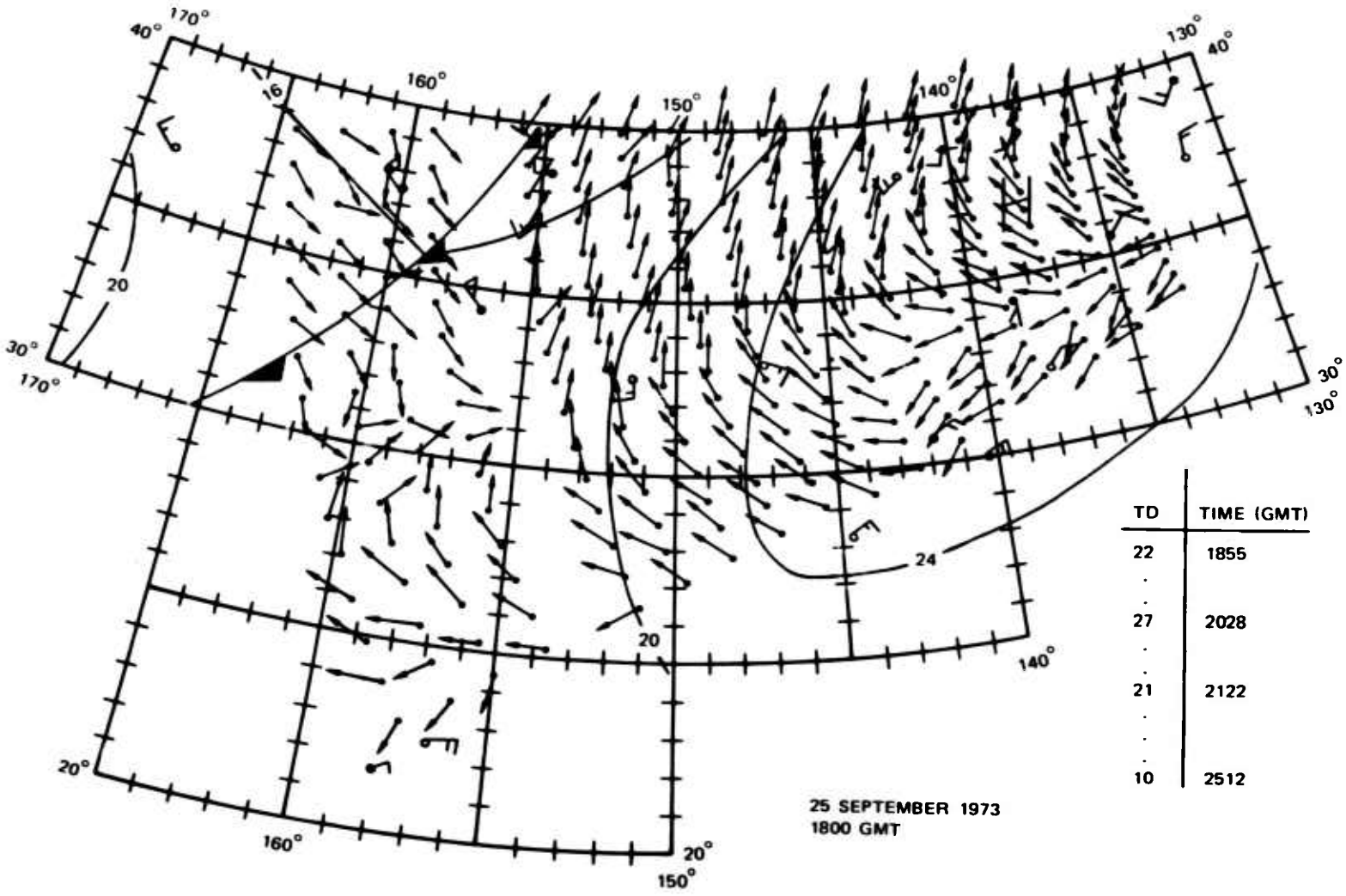


FIGURE 6 RADAR WEATHER MAP FOR 25 SEPTEMBER 1973, COMPARED TO THE NWS ANALYSIS OF 1800 GMT ON THE SAME DAY. The radar winds represented are for times between 1800 and 2400 GMT. Wind direction is plotted by arrows; the feet of the arrows denote positions. Wind circulation generally agrees well with the weather map. The cold front detected by the radar does not agree, however.

The ESSA-VII cloud photograph taken near 1800 GMT is shown in Fig. 7 for comparison to Fig. 6. The cold front is identified by a well-developed elongated bright band of clouds oriented NE/SW extending through 40°N, 150°W. The cellular-appearing clouds between 140°W and 130°W and near 30°N are characteristic of clouds around the southwestern perimeter of an oceanic high-pressure area ahead of a well developed cold front. The center of the high-pressure area is located somewhere in the clear area in the right-hand edge of the photograph (Fig. 7).

The general agreement between the radar-derived wind fields and the independent surface-wind measurements on 25 September was good. The cold front position shown in Fig. 6 was plotted by NWS approximately 200 nmi to the northwest of the front indicated by the radar data. The radar-inferred wind shifts agree with the wind shifts implied by the satellite cloud photograph displaying and locating the frontal cloud cover. The discontinuous nature of the wave field recorded by the radar is a good method for detailing the position of the front and the wind field across the front.

The radar-derived wind field for the second day, 26 September 1973, is shown in Fig. 8, and the corresponding cloud photograph in Fig. 9. The radar winds showed the frontal wind discontinuity very clearly, as well as a wind discontinuity associated with a trough in the easterlies west of 155°W and proximal to 25°N (Fig. 8). With the exception of poor data at 18 ms delay (not plotted), the quality of the radar data was much improved over the first day. This improvement was attributed to the earlier starting time on the second day, which yielded better ionospheric propagation. Since the radar data on the second day were recorded between the hours of 1620 GMT and 2003 GMT, the wave directions plotted should be applicable for mean winds blowing between the hours of about 1550 GMT and 1930 GMT, respectively.

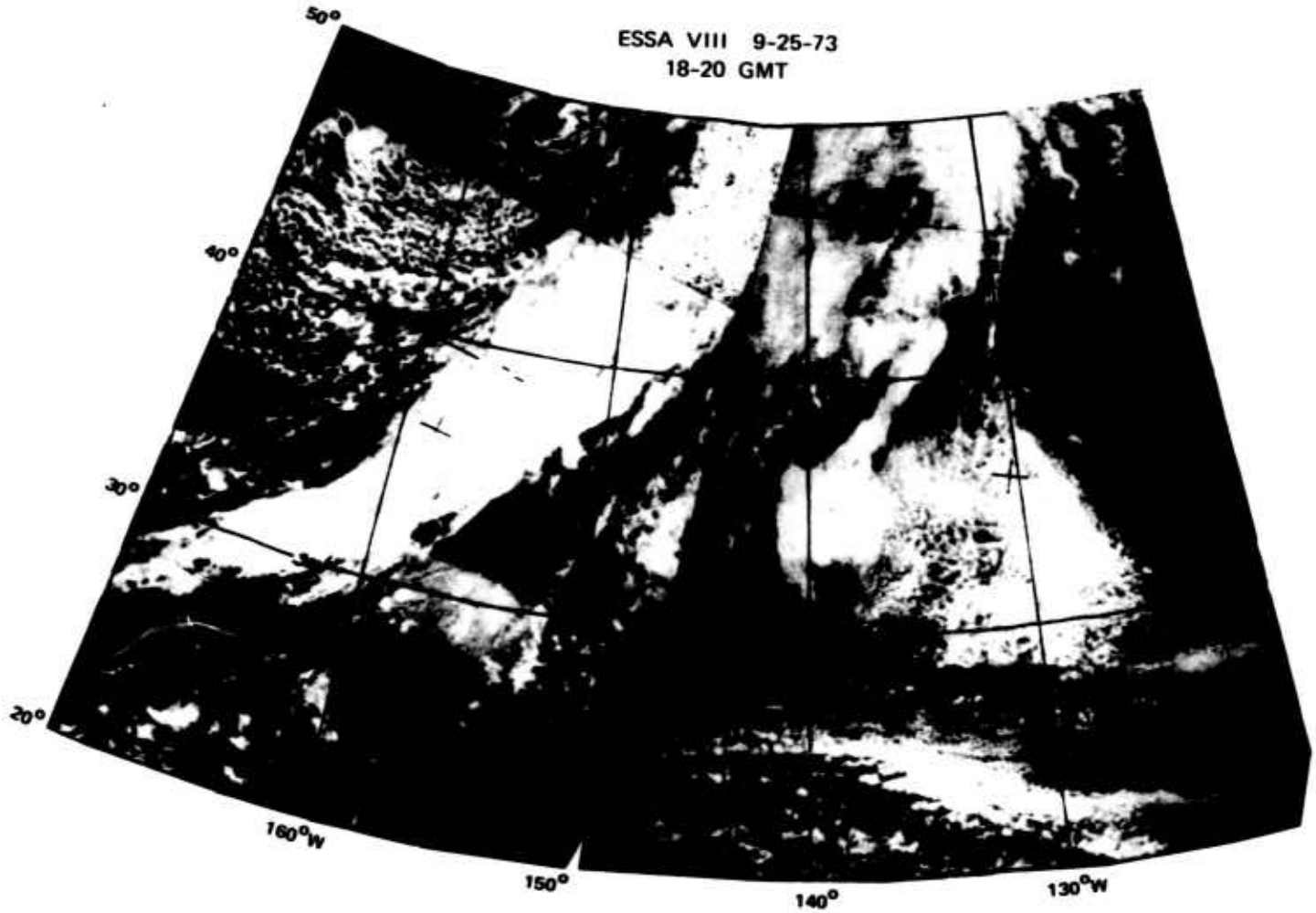


FIGURE 7 ESSA VIII CLOUD PHOTOGRAPH OVER THE SCATTERING AREA ON THE MORNING OF 25 SEPTEMBER 1973. Note the cold front on the left and the high-pressure zone near 35°N, 139°W.

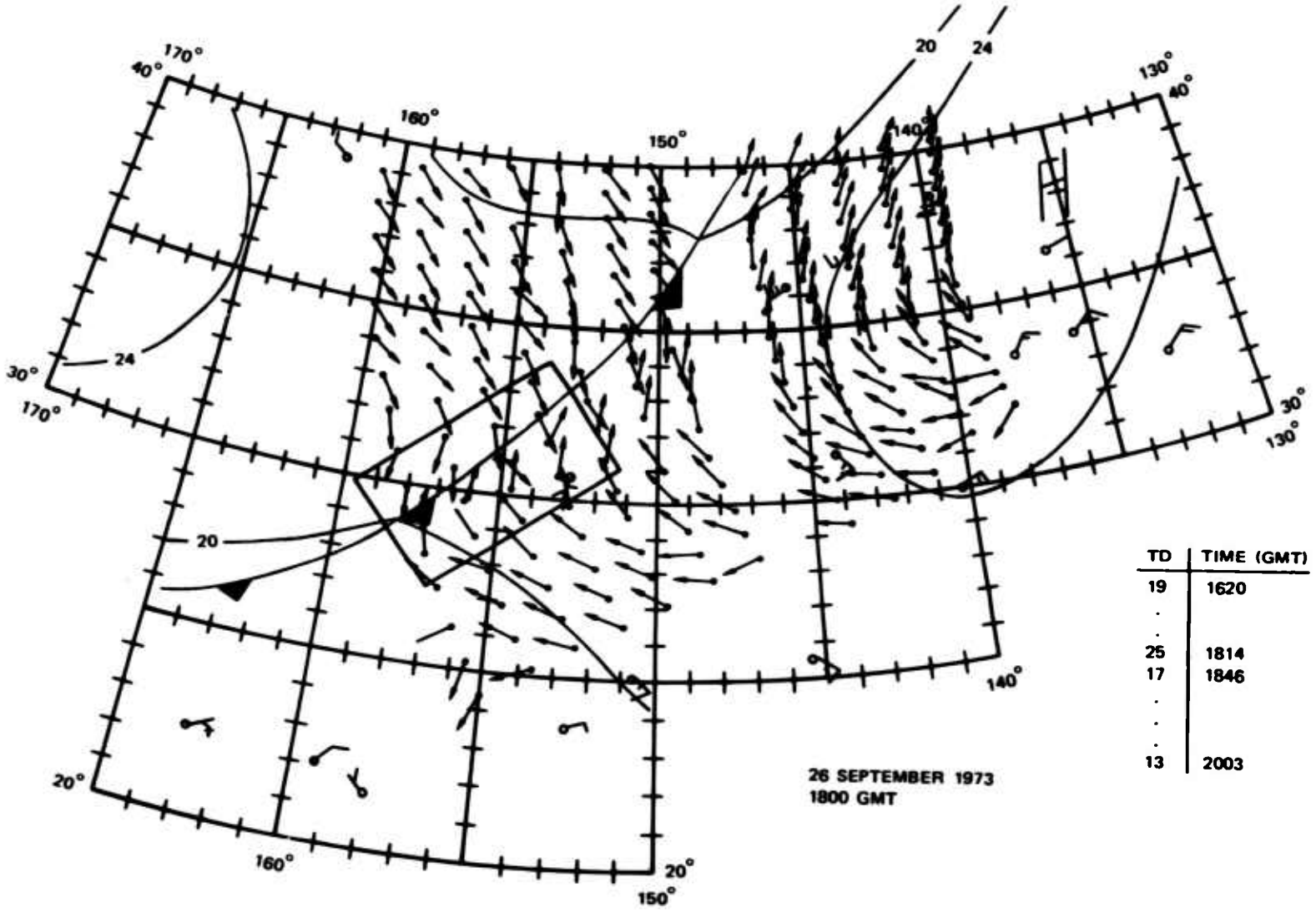


FIGURE 8 RADAR WEATHER MAP FOR 26 SEPTEMBER 1973 COMPARED TO NWS MAP AT 1800 GMT (similar to Fig. 6). The radar data reflected winds blowing between the hours of 1530 and 1900 GMT. Almost all of the data agree well with ship-measured winds and the NWS-assumed location of the cold front and high-pressure center (see text).

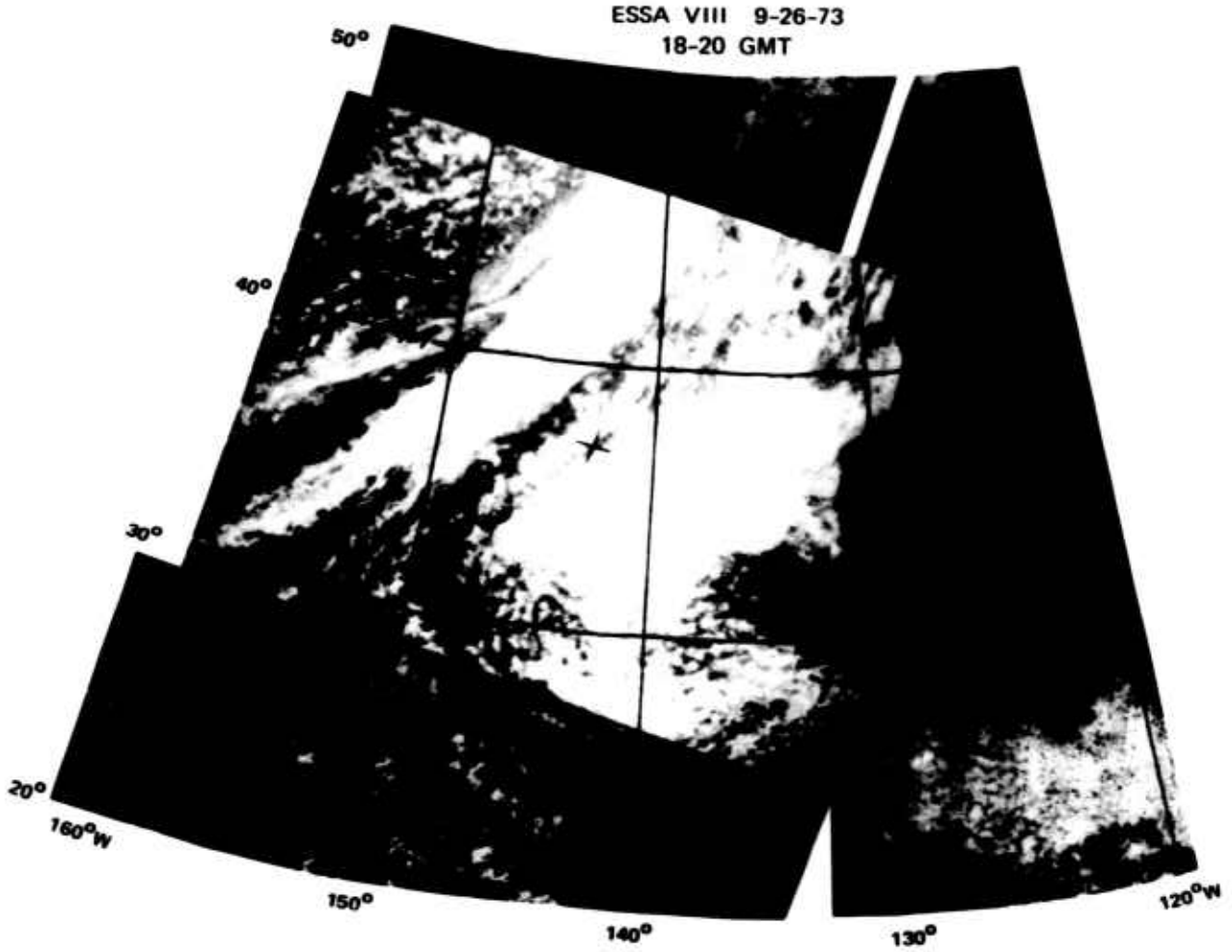


FIGURE 9 ESSA VIII CLOUD PHOTOGRAPH OVER THE SCATTERING AREA ON THE MORNING OF 26 SEPTEMBER 1973. Note the cold front on the left and the high-pressure zone near 35°N, 139°W.

The magnitude of the wind was added to the direction vectors in the area outlined on Fig. 9 in the vicinity of the cold front. The method described by Stewart and Barnum [7], with the improvements illustrated by Maresca and Barnum [8], was used. The results are illustrated in Fig. 10.

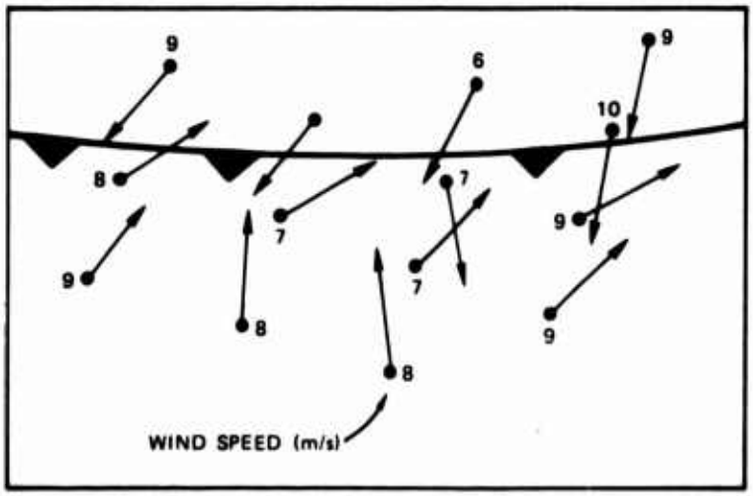


FIGURE 10 WIND SPEED, IN METERS PER SECOND, AND DIRECTION ARROWS IN THE VICINITY OF THE ATMOSPHERIC FRONT ON 26 SEPTEMBER 1973

## VII CONCLUSIONS

The most important contribution found in this experiment was the ability to detect the abrupt wind shifts across the cold front. Thus, when rapid spatial variations in wind fields occur, the high-frequency sea waves will also respond rapidly and this response can be detected by the radio scatter. High spatial resolution was thus essential for the detection of these abrupt wind direction changes. In one example illustrated herein, a 16° shift occurred over only a half degree of radar azimuth, equivalent to about 1.5 km in cross range. Range resolutions of comparable size are essential to the analysis of atmospheric fronts and

the gradient of wind stress across intense cyclones. Resolutions of 3 km are readily achievable with the WARF radar.

Over 90% of high-resolution sea backscatter Doppler spectra recorded on these two successive days over an area exceeding $3 \times 10^6$ $(km)^2$ were readily usable for calculation of the mean oceanic wind direction. Due to ionospheric perturbation of the echoes, a lesser number could be used for calculation of wind speed.

Ionospheric conditions varied both in space and time. These variations were not abnormal. Multipath was most severe at ranges exceeding 3000 km. This limitation was reduced by recording data at the longer ranges earlier in the day. It is clear that the percentage of data usable for wind speed can be increased by matching radar parameters to ionospheric skip parameters at each observation point. For example, a north-south azimuth scan at a constant radio frequency should incorporate a variable time-delay (range) gate to match north-south tilts in ionospheric electron density.

A variety of applications are evident for the remote sensing of wind fields by OTH radar. The capability for measuring the mean wind field combined with a high-resolution capability for detecting abrupt shifts in consistent winds, should lead to a significant capability for tracking and surveying hurricanes.

Future work will be centered on radar data analysis with good ground truth under a variety of conditions, and on the development of improved processing and operating techniques in light of ionospheric variations.

## REFERENCES


1. A. E. Long and D. B. Trizna, "Mapping of North Atlantic Winds by HF Radar Sea Backscatter Interpretation," IEEE Trans. on Antennas and Propagation, Vol. AP-21, No. 5, pp. 680-685 (September 1973).

2. T. A. Croft, "Sky-Wave Backscatter: A Means for Observing our Environment at Great Distances," Reviews of Geophysics and Space Physics, Vol. 10, No. 1, pp. 73-155 (February 1972).

3. D. E. Barrick, J. M. Headrick, R. W. Bogle and D. D. Crombie, "Sea Backscatter at HF: Interpretation and Utilization of the Echo," Proceedings of the IEEE, Vol. 62, No. 6, pp. 673-680 (June 1974).

4. J. L. Ahearn, S. R. Curley, J. M. Headrick and D. B. Trizna, "Tests of Remote Skywave Measurement of Ocean Surface Conditions," Proceedings of the IEEE, Vol. 62, No. 6, pp. 681-687 (June 1974).

5. G. L. Tyler, C. C. Teague, R. H. Stewart, A. M. Peterson, W. H. Munk, and J. W. Joy, "Wave Directional Spectra From Synthetic Aperture Observations of Radio Scatter," Deep-Sea Research, Vol. 21, pp. 989-1016 (1974).

6. D. L. Johnstone, "Second-Order Electromagnetic and Hydromagnetic Effects in High-Frequency Radio-Wave Scattering from the Sea," Technical Report No. 3615-3 (SEL-75-004) (Ph.D. Dissertation), Stanford Electronics Laboratories, Stanford, Calif. (March 1975).

7. R. H. Stewart and J. R. Barnum, "Radio Measurements of Oceanic Winds at Long Ranges: An Evaluation," Radio Science, Vol. 10, No. 10, pp. 853-857 (October 1975).

8. J. W. Maresca, Jr., and J. R. Barnum, "Measurement of Oceanic Wind Speed From HF Sea Scatter by Skywave Radar," accepted for publication in IEEE Trans. on Antennas and Propagation, Vol. AP-25, No. 1 (January 1977).

9. R. A. Shepherd and J. B. Lomax, "Frequency Spread in Ionospheric Radio Propagation," IEEE Trans. on Communication Technology, Vol. COM-15, No. 2, pp. 268-275 (April 1967).

10. M. S. Longuet-Higgins, D. E. Cartwright, and N. D. Smith, "Observations of the Directional Spectrum of Sea Waves Using Motions of a Floating Buoy," Ocean Wave Spectra, pp. 111-136 (Prentice-Hall, Inc., Englewood Cliffs, N.J., 1963).

11. J. M. Headrick and M. I. Skolnik, "Over-the-Horizon Radar in the HF Band," Proc. IEEE, Vol. 62, No. 6, pp. 664-673 (June 1974).

12. J. R. Barnum, "Skywave Polarization Rotation in Swept-Frequency Sea Backscatter," Radio Science, Vol. 8, No. 5, pp. 411-423 (May 1973).

13. W. F. Marshall and J. R. Barnum, "Measurement of Sea Scatter and Buoy Tracks at Long Ranges by High-Resolution OTH-B Radar," Technical Report 1 (NR 083-320), Stanford Research Institute, Menlo Park, Calif. (May 1975).

Appendix B

# MEASUREMENT OF OCEANIC WIND SPEED FROM HF SEA SCATTER BY SKYWAVE RADAR

by

Joseph W. Maresca, Jr.
and
James R. Barnum, Member IEEE

Accepted for Publication in
IEEE Transactions on Antennas and Propagation
(Special Issue on Radio Oceanography)

September 1975

This work was performed by Stanford Research Institute, Menlo Park, California, and was sponsored in part by the Office of Naval Research and the National Science Foundation as part of the North Pacific Experiment (NORPAX).

Appendix B

# MEASUREMENT OF OCEANIC WIND SPEED FROM HF SEA SCATTER BY SKYWAVE RADAR


## ABSTRACT

Remote measurements of the spatial mean ocean wind speeds were obtained using Doppler spectra resolved to 0.08 Hz from high-resolution HF skywave-radar backscatter measurements of the ocean surface. A standard deviation of 2.4 m/s resulted from the correlation of observed winds over the ocean and the broadening of the Doppler spectra in the vicinity of the higher first-order Bragg line. This broadening, for Doppler spectra unperturbed by the ionospheric propagation, is proportional to the increase in power caused by higher-order hydrodynamic and electromagnetic effects in the vicinity of the Bragg line and inversely proportional to the square root of the radio frequency. A lower bound on the measure of wind speed was established at 5 m/s by the low-resolution spectral processing and low second-order power. An upper limit is suggested by the steep slope in the region of the sea backscatter spectrum outside the square root of two times the first-order Bragg line.


## I INTRODUCTION

High-resolution HF OTH-B radar measurement of ocean surface winds over large areas of ocean are important to the study of large-scale air/sea energy exchanges. Empirical estimates of the ocean surface wind are an indirect measurement based on the ocean wave field which acts as a scattering surface. Theoretical models of the hydrodynamic and electromagnetic contributions to the backscatter Doppler spectrum and their comparison with data obtained from HF surface-wave radar have been published by Barrick [1], and Johnstone [2]. The surface roughness

is represented by an assumed form of the ocean wave spectrum. If the assumed functional form of the wave spectrum results in a good fit between the model of the Doppler spectrum and the measured Doppler spectrum, then sea state is predictable. For fully developed conditions, the match between the theory and the measured return is good. Using the second-order theory, Johnstone correlated wind speed with the ratio of the second-order power to the first-order power. Simpler determinations of wind speed from empirical correlations based on the second-order theory have been developed by Ahearn et al. [3] and Stewart and Barnum [4]. Ahearn et al. correlated the increase in power measured at the lowest level between the Bragg lines with the wind speed, and Stewart and Barnum correlated the increase in the -10 dB spectral width of the Doppler spectrum, defined as B, in the vicinity of the higher Bragg line.

The objectives of this paper are to report an improvement in the correlation of B with wind speed, originally presented by Stewart and Barnum, by accounting for a difference in radar operating frequencies, and to discuss the accuracy of the technique.

## II THEORETICAL CONSIDERATIONS AND DATA NORMALIZATION

The wind speed obtained from the spectral broadening in the vicinity of the stronger Bragg line is a spatial average of the mean wind required to generate the waves in a given area of ocean at the time of the radar backscatter measurement; it is not a measure of the instantaneous wind. B is a measure of this spectral broadening on data processed with 12.8 s of coherent integration with cosine-squared weighting on the received waveform. It was defined [4] as the width of the Doppler spectrum 10 dB down from the maximum Bragg line power. At this spectral resolution (0.078 Hz), the higher-order contributions are separate [Fig. 1(a)],

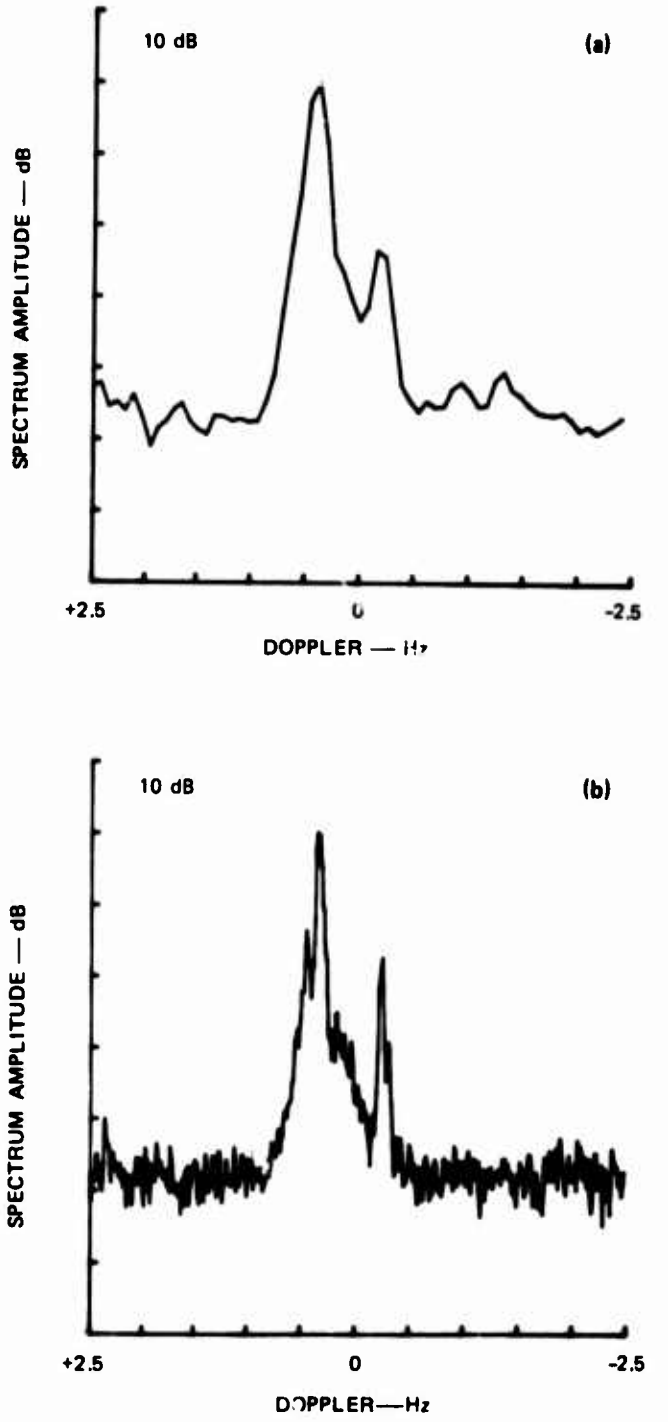


FIGURE 1 EXAMPLE OF DOPPLER SPECTRA COHERENTLY INTEGRATED FOR (a) 12.8 s AND (b) 102.4 s FOR A GIVEN RADAR DWELL

but not uniquely resolvable from the Bragg-line power [Fig. 1(b)]. The spectral broadening in this region has been shown [1],[2] to be a function of the higher-order electromagnetic and hydromagnetic effects of scattering from the ocean surface. It is probable that the increase in second-order power in the Doppler spectrum is a result of the low-frequency portion of the wave spectrum. This is suggested by a comparison of the second-order power obtained from the form of the ocean wave spectrum suggested by Phillips [5], which has a vertical low-frequency cutoff that eliminates the energy contribution at the lower frequencies, with the form of the ocean wave spectrum suggested by Pierson and Moscowitz [6], which includes the energy at these lower frequencies.

The resonant Bragg scatter amplitude from particular ocean waves (Doppler = $\sqrt{n}\ \Delta f_1$, where n = 1, 2, 3, 4 ...) saturates at particular wave heights and no further increase in power is experienced. For example, sustained winds greater than 12 m/s will saturate the scatter for n = 1, 2, and 3 above a frequency of 10 mHz. However, second-order contributions in the region between zero Doppler and the Bragg line ($\Delta f_1$) and between the Bragg line and the $2^{3/4}\ \Delta f_1$ increase with increasing surface roughness and are particularly sensitive to increasing wind speeds [2]. The theory shows that the increase in power between $\Delta f_1$ and $\sqrt{2}\ \Delta f_1$ is a function of wind direction and wind speed. The greatest increase in second-order power is found close to the Bragg line as the wind speed increases. For low wind speeds, less than about 5 m/s, second-order contributions near the Bragg line are negligible. For high wind speeds, the second-order power contributions continue to increase in the region between the Bragg line and $\sqrt{2}\ \Delta f_1$. The second-order theory shows that contributions between the positive and negative first-order Bragg lines are more a function of wind direction and do not increase significantly with wind speed at a given direction. The scatter at Dopplers higher than the second-order contribution at

$2^{3/4}\,\Delta f_1$ is not sensitive to an increase in surface roughness [2] and is therefore not a good measure of sea state and therefore wind speed.

The Doppler frequencies of the Bragg line and surrounding second-order singularities are inversely proportional to the square root of the radio frequency. Thus, the Doppler width of second-order scatter between $\Delta f_1$ and $2^{3/4}\,\Delta f_1$ will exhibit a functional dependence that is also proportional to the inverse of the square root of frequency. Also, as evident in Barrick et al. [7], the magnitude of the second-order scatter relative to the first-order Bragg line will increase with increase in the radio frequency at a constant wind speed. The relative position of the second-order peak also changes; thus, it is not yet clear how the overall frequency dependence is affected.

The Bragg line can be normalized to unity by dividing through the Doppler spectrum by

$$\sqrt{f_o \frac{g}{\pi c}}$$

where f is the radio frequency, g is the acceleration due to gravity, and c is the speed of light. Since $g/\pi c$ is a constant and since the mean frequency of the data is approximately 20 MHz, the data were normalized by $(20/f_o)^{1/2}$, where $f_o$ is the radio frequency in MHz.

## III DATA ANALYSIS AND RESULTS

The HF OTH-B measurements were taken as part of both the NORPAX experiment [4] and other experiments using the Wide Aperture Research Facility described by Barnum [8] and Barnum et al. [9]. The Doppler spectrum used in the B measurement was obtained by incoherently averaging 40 Doppler spectra over a scattering patch of 15 km by 60 km for 12.8 s of coherent integration. Five adjacent areas of ocean (Fig. 2) separated

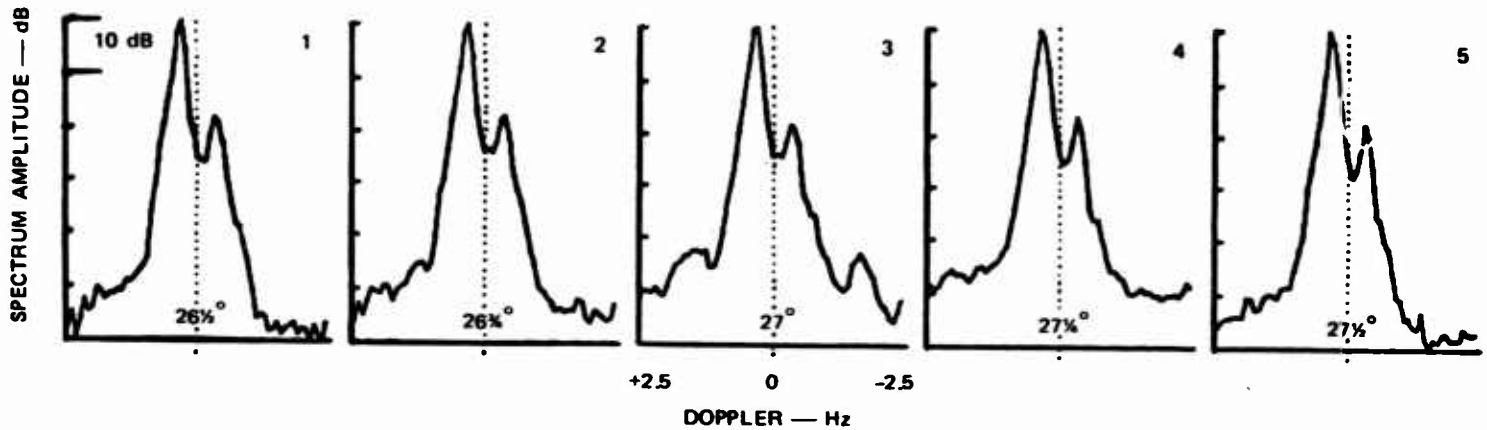


28 FEBRUARY 1975
1659:48 GMT
FREQUENCY 11.445-11.465
IDOP 0.156
TIME DELAY 12.500 ms
MAPS AVERAGED = 1
LATITUDE 28.51 LONGITUDE 136.58

| AZIMUTH | X (dB) | B (Hz) |
|---|---|---|
| 1 | 17.6 | 0.345 |
| 2 | 17.7 | 0.338 |
| 3 | 16.9 | 0.352 |
| 4 | 15.2 | 0.372 |
| 5 | 15.5 | 0.366 |
| AVG | 16.7 | 0.354 |

**FIGURE 2** EXAMPLE OF THE REAL-TIME BACKSCATTER DISPLAY USED FOR RECORDING DATA FOR WIND-FIELD MAPPING. Each such display is updated once per minute at a new ocean location. Five different azimuths are displayed with the numerical values of X and B for each azimuth displayed in the lower right-hand table.

by one-quarter degree were simultaneously processed in real time. Only spectrally pure ionospheric propagation data were analyzed and only the minimum B out of the five spectra was selected to use in the correlation.

The observed wind speeds were obtained from Research Vessel Flip, U.S. Navy ships, and ships of opportunity; therefore, the accuracy of the values of wind speed observed in situ will differ. The accuracy may range from 0.5 m/s to over 2.0 m/s, and depends on the accurate determination of the ship's speed, the precision and calibration of the anemometer, and the length of the wind record used to obtain an average value.

The data set is presented in Table 1 and includes a subset of the data in [4]. To eliminate bias in the correlation, only one B at each geographical location was selected for an observed wind on any given day, and no more than three points for any given storm.

A least-squares fit was made to the scatter diagram of the unnormalized B and observed wind speed for all radar frequencies. The resulting standard deviation was 3.5 m/s, similar to [4]. As noted above, much of the standard deviation can be accounted for by the differences in radar frequency associated with each B value.

The data were normalized by $(20/f_o)^{1/2}$, and are plotted in Fig. 3. The least-squares fit to these points is

$$U = 33B' - 2 \qquad (1)$$

where

$$B' = (20/f_o)^{1/2} B$$

and U is the wind speed in m/s. The correlation coefficient is 0.8, and the standard deviation is 2.4 m/s. The previous influence of the higher wind speeds on the regression fit is not significant. The

Table 1

RAW DATA USED IN CORRELATION OF B AND WIND SPEED

| Number | Broadness, B (Hz) | Wind Speed, U (m/s) | Radar Frequency, $f_o$ (MHz) |
|---|---|---|---|
| 1 | 0.29 | 8.5 | 25.6 |
| 2 | 0.39 | 8.2 | 21.5 |
| 3 | 0.35 | 3.6 | 23.0 |
| 4 | 0.32 | 5.1 | 20.7 |
| 5 | 0.30 | 7.1 | 20.7 |
| 6 | 0.33 | 7.7 | 18.6 |
| 7 | 0.33 | 8.0 | 20.1 |
| 8 | 0.34 | 6.2 | 19.5 |
| 9 | 0.33 | 7.2 | 21.7 |
| 10 | 0.60 | 18.0 | 19.0 |
| 11 | 0.58 | 21.0 | 20.3 |
| 12 | 0.54 | 15.0 | 21.6 |
| 13 | 0.35 | 12.3 | 11.5 |
| 14 | 0.42 | 13.4 | 15.8 |
| 15 | 0.34 | 11.8 | 17.5 |
| 16 | 0.32 | 12.6 | 15.8 |
| 17 | 0.28 | 12.9 | 6.2 |
| 18 | 0.28 | 8.5 | 20.7 |
| 19 | 0.24 | 10.3 | 8.2 |
| 20 | 0.30 | 7.7 | 21.9 |
| 21 | 0.28 | 10.3 | 21.9 |
| 22 | 0.28 | 10.3 | 13.9 |
| 23 | 0.30 | 12.9 | 14.7 |
| 24 | 0.34 | 7.7 | 14.8 |
| 25 | 0.34 | 7.7 | 13.9 |

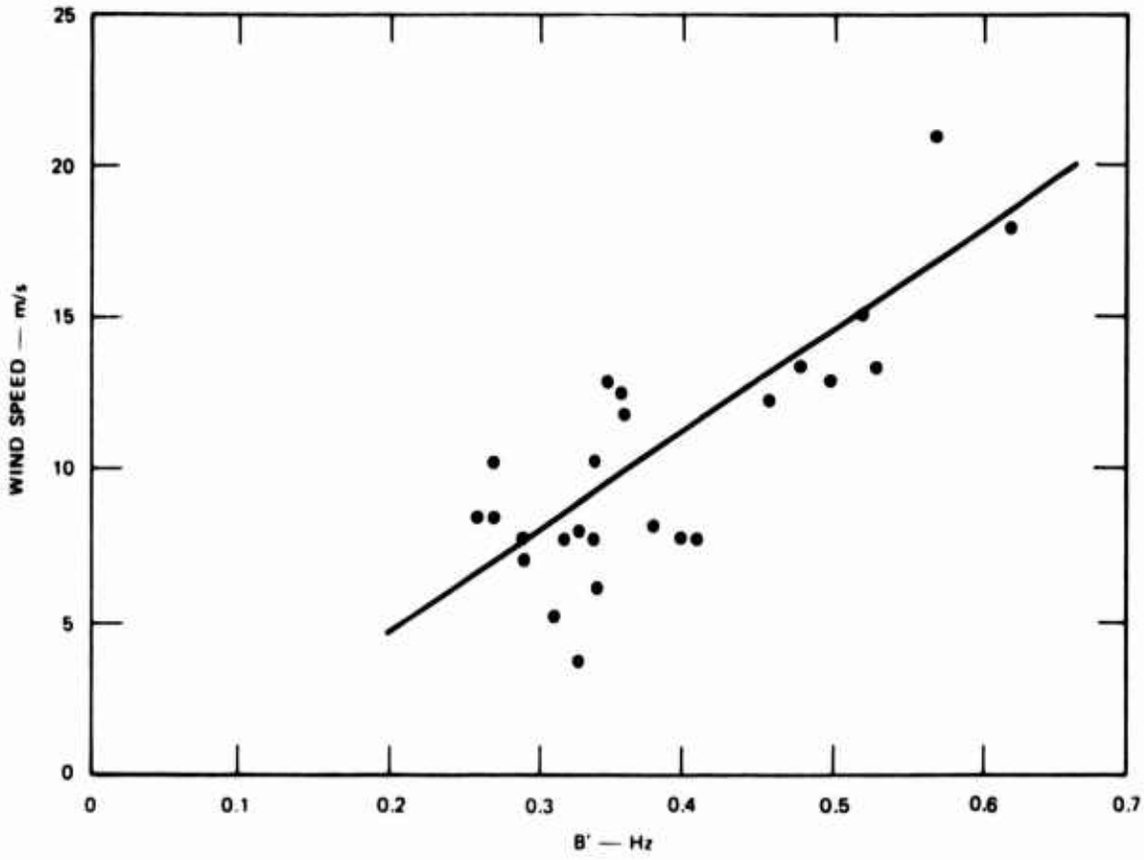


FIGURE 3 CORRELATION OF WIND SPEED WITH SPECTRUM BROADENING

accuracy of the estimate of wind speed using Eq. (1) is on the same order of magnitude as the ship of opportunity reports presently used to obtain the wind field over a large area of ocean.

## IV DISCUSSION OF ACCURACY

The accuracy of this correlation is dependent on the natural variability of the instantaneous wind field, the accuracy of the winds measured in situ, the fetch and duration of sustained winds, and various forms of spectral broadening in the vicinity of the first-order Bragg line that may not be related to the local winds at the scattering area.

## A. Natural Wind Variability

The standard deviation of the actual instantaneous wind speed will vary from region to region, but is usually assumed greater in the temperate zones than in the tropical zones where the trade winds are approximately constant for long time periods. If the wind is not uniform over the scattering area, the observed wind, a point-source measurement, will not be representative of the spatially averaged wind speed obtained by radar measurements. In addition, the instrumentation used to measure the winds in situ will possess its own source of error. Measurements from a moving platform will be less accurate than from a stationary platform. Errors may be as great as 2 m/s. The standard deviation of the observed wind field determined from measurement error and the natural wind field variability define the minimum acceptable accuracy of our correlation.

## B. Fetch and Duration

The inference of the mean wind field by ocean wave scatter using B is dependent on fetch and duration [4] as well as wind speed. Since it is assumed that the mean wind field to generate the ocean surface is the mean wind averaged over that same time period, only a fully developed sea will give a unique result. The data are insufficient to determine if a 20 m/s wind was blowing for 1 hour or if a 8 m/s wind was blowing for 17 hours, over a constant fetch at the time of the backscatter measurement. It appears that the measure should be strictly valid only for a fully developed sea. Since wave growth is not considered in the correlation, B should continue to increase until the sea is fully developed or at its maximum energy state for the wind system. If too few values of B are obtained in a given area, one cannot ensure that B has reached its maximum value. This should be responsible for some of

the scatter in Fig. 3. We believe that several values of B should be measured over time on the order of hours, and that the maximum value of B, coincident with clean propagation, should be selected. It could then be assumed that the measured B has approached the B of a fully developed sea.

## C. Unwanted Spectral Broadening

Remaining potential errors result from unwanted spectral broadening in the vicinity of the higher first-order Bragg line. These include ionospheric multipath and fine-scale motion, the possible influence of swell and diverging (converging) currents, and the degree of statistical fluctuation of the spectral components in the sea scatter.

All OTH-B data are subject to ionospheric perturbation, and only backscatter data free of the effects of multipath and fine-scale ionospheric motion in the region of the B measurement can be meaningfully analyzed. Five common ionospheric perturbations to the Doppler spectrum are shown in Fig. 4: (a) insufficient signal strength; (b) multipath outside the B region; (c) multipath inside the B region; (d) multipath in the B region not easily distinguishable; and (e) fine-scale motion in the B region (not shown). If the multipath does not interfere with the measurement of B [Fig. 3(b)], then the measurement can still be achieved. Only the return where obvious broadening has occurred but no multipath is visible presents difficulty [Fig. 3(d)]. The five-azimuth display aids in assessment. In this case, the Doppler spectra on adjacent azimuths have obvious multipath [Fig. 3(d)] and it must be concluded that the center spectrum is contaminated and unsuitable for analysis. This problem is minimal in the correlation leading to (1), since only clean spectra were used. To minimize ionospheric broadening shown in Fig. 4(e), only the minimum value of B was selected for analysis from many Doppler spectra taken in a region at each time period.

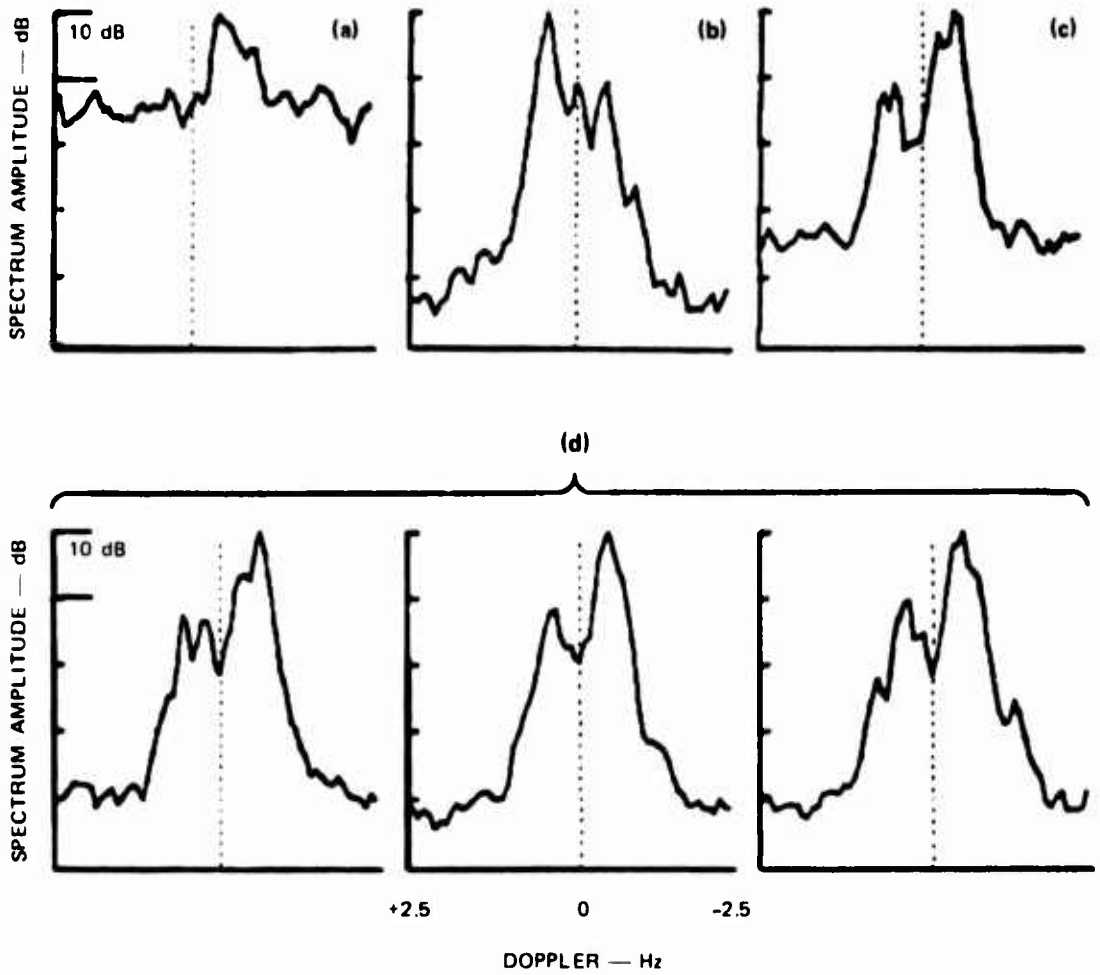


FIGURE 4 EXAMPLES OF DOPPLER SPECTRA. (a) Insufficient signal strength. (b) Multipath (two paths) that does not affect the measurement of B. (c) Multipath (two paths) that affects the measurement of B (Hz). With further processing, the effects of the unwanted path might be subtracted to obtain a clean Doppler spectra. (d) Multipath in the adjacent Doppler spectra, simultaneously recorded on adjacent azimuths, indicating that the broadening in the center Doppler spectrum is due to ionospheric motion.

Spectral broadeining of the Bragg line might also occur from swell [4], and from diverging or converging surface currents within the scattering patch. Coherent scatter from swell [2] appears at Dopplers well removed from the Bragg line at 10 MHz (and higher), and therefore such scatter would not broaden the spectra. Modulations of the first-order scatter by large swell was not considered a source of error in [4]. The narrow beam (1/3°) of the WARF radar minimizes the possibility of diverging or converging currents occurring in the scattering area; however, such currents could produce serious misinterpretation of the data for larger antenna beamwidths.

To eliminate statistical variation in the spectr due to random sea scatter amplitudes, the experimental data were analyzed to determine the optimal tradeoff among spatial averaging, and coherent and incoherent spectrum integration. The ratio of the approach and recede first-order Bragg lines defined as X [9] was used as the parameter of the test. Using a data record of up to 256 s, the analysis proceeded for 102, 51, 26, and 13 s of coherent integration, and 1, 2, 4, 8, 12, 16, and 20 incoherent averages for various coherent integration times. It was found that longer coherent integration time increased spectral resolution but did not reduce statistical scatter. Incoherent averaging of the spectra reduced the scatter (as would be expected for this assumed Gaussian process). Based on the results of this analysis (Fig. 5), it was concluded that four to eight incoherent averages are required per range line regardless of the coherent integration time. The incoherent spatial average of the backscatter measurements must be increased for decreased incoherent averaging.

It is concluded that the scatter in the data reported here is due primarily to the natural variability of the mean wind field, and the error in the in situ measurement of the observed winds (particularly for the higher wind values).

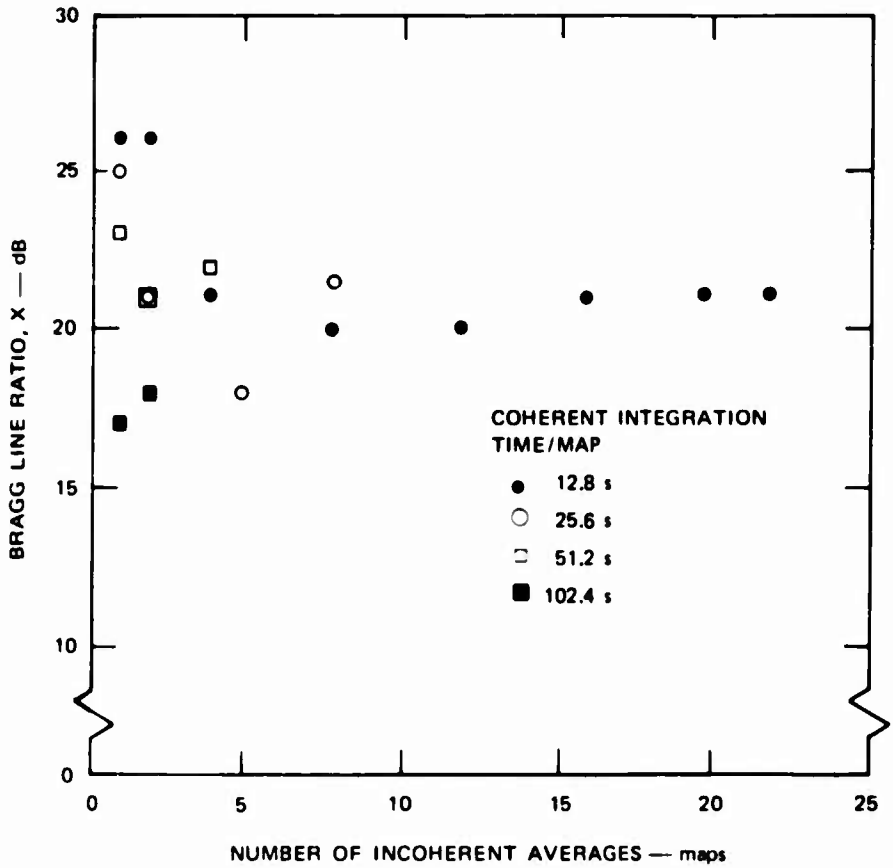


FIGURE 5 THE EFFECT OF INCOHERENT AVERAGING ON OBTAINING A MEAN VALUE FOR X. Doppler spectra coherently integrated for 12.8, 25.6, 51.2, and 102.4 s were averaged to obtain a mean value of X. The mean value of X ± 1 dB is approached for 4 to 8 incoherent averages (maps).

## V RANGE OF B

A minimum value of B is determined by the processing. According to our present automatic measure of B with a 12.8-s integration, its minimum value for no second-order contribution ranges from 0.197 Hz to 0.225 Hz, depending on the location of the first-order Bragg line relative to the nearest Doppler cell generated by the FFT. These minimum values of B above were calculated for the Bragg line centered on a Doppler cell and located midway between Doppler cells, respectively. A B of 0.2 Hz corresponds to a wind speed of 5 m/s at 20 MHz (Fig. 3). Choosing the minimum value of B from a number of relatively closely spaced samples following

unperturbed propagation tends to result in selection of Doppler spectra in which the Bragg line is centered or is close to centered on a Doppler cell.

At the other extreme, the theoretical spectra calculated by Johnstone [2] suggest an upper limit on the wind-speed calculation using B. As the wind speed increases, the power in the spectral peak found at $\sqrt{2}\ \Delta f_1$ also increases. If this peak saturates below -10 dB the linear approximation on which the correlation is based is reasonable. When this peak saturates above -10 dB, B increases only very slowly with increasing wind, due to the steep slope of the region outside this spectral component, and the linear approximation to U(B) will become invalid. Although B will continue to increase with increasing wind speed, this increase will not be detectable by this method.

## VI CONCLUSION

The spectral broadening in the vicinity of the first-order Bragg line at a constant sea state is a function of the radio frequency. One factor of this function is inversely proportional to the square root of frequency. Normalizing the data by $f_o^{-1/2}$ resulted in a standard deviation of 2.4 m/s, which is equal to the ship of opportunity data. The correlation is valid for wind speeds greater than 5 m/s at 20 MHz (Fig. 3); an upper wind-speed limit is suggested by theory, but is unknown. The lower limit is determined by the minimum spectral width possible in the spectral processing and the negligible second-order contributions near the first-order Bragg line for winds less than 5 m/s. The use of B to infer oceanic winds is particularly suited to covering large ocean areas in detail, since only 12.8 s of coherent integration are required for the measurement. It is especially noteworthy that the relatively low wind-speed error (2.4 m/s) was found using B, even though winds

from 5 to 25 m/s were observed, and the fetch and duration of the winds were unknown. Further work will confirm whether or not this was pure coincidence.

## REFERENCES


1. D. C. Barrick, "Remote Sensing of Sea State by Radar" in Remote Sensing of the Troposphere, V. E. Derr, ed., Washington, D.C., U.S. Government Printing Office, Chapter 12, 1972.

2. D. L. Johnstone, "Second-Order Electromagnetic and Hydromagnetic Effects in High-Frequency Radio-Wave Scattering from the Sea," Technical Report No. 3615-3 (SEL-75-004) (Ph.D. Dissertation), Contracts N00014-75-C-0356 and N00014-69-A-0200-6012, Stanford Electronics Laboratories, Stanford, California, March 1975.

3. J. L. Ahearn, S. R. Curley, J. M. Headrick and D. B. Trizna, "Tests of Remote Skywave Measurement of Ocean Surface Conditions," Proc. IEEE, Vol. 62, No. 6, pp. 681-687, June 1974.

4. R. H. Stewart and J. R. Barnum, "Radio Measurements of Oceanic Winds at Long Ranges: An Evaluation," Radio Science, Vol. 10, No. 10, pp. 853-857, October 1975.

5. O. M. Phillips, "The Equilibrium Range in the Spectrum of Wind-Generated Ocean Waves," J. Marine Res., Vol. 16, pp. 231-245 (1958).

6. W. J. Pierson, Jr. and L. Moscowitz, "A Proposed Spectral Form for Fully Developed Wind Seas Based on the Similarity Theory of S. A. Kitaigordskii," J. Geophys. Res., Vol. 69, No. 24, pp. 5181-5190 (1964).

7. D. E. Barrick, J. M. Headrick, R. W. Bogle and D. D. Crombie, "Sea Backscatter at HF: Interpretation and Utilization of the Echo," Proc. IEEE, Vol. 62, No. 6, pp. 673-680, June 1974.

8. J. R. Barnum, "Skywave Polarization Rotation in Swept-Frequency Sea Backscatter," Radio Science, Vol. 8, No. 5, pp. 411-423, May 1973.

9. J. R. Barnum, J. W. Maresca, Jr., S. M. Serebreny, "High-Resolution Mapping of Oceanic Wind Fields with Skywave Radar," accepted for publication in IEEE Trans. on Antennas and Propagation, Vol. AP-25, No. 1 (January 1977).

Appendix C

# MEASUREMENT OF AN OCEAN WAVE SPECTRUM BY HF SKYWAVE RADAR

by

Joseph W. Maresca, Jr.
Donald L. Johnstone
James R. Barnum

To be Submitted for Publication in
Journal of Geophysical Research

December 1975

This work was performed by Stanford Research Institute, Menlo Park, California, and was sponsored by the Office of Naval Research and the National Science Foundation as part of the North Pacific Experiment (NORPAX).

Appendix C

# MEASUREMENT OF AN OCEAN WAVE SPECTRUM BY HF SKYWAVE RADAR


## ABSTRACT

An ocean wave spectrum for the North Pacific Ocean (29°N, 137°W) was inferred from sea backscatter measurements taken by HF skywave radar on 12 February 1975. A trial-and-error solution was used to estimate this spectrum by comparing a theoretical second-order radio-wave scattering model of the Doppler spectrum, produced by assuming an ocean wave spectrum, to the observed Doppler spectrum until a match was found. The comparison of the final calculated Doppler spectrum and the measured Doppler spectrum showed fair agreement. The significant wave height derived using this technique agreed to within ten percent of the in situ observations of the wave height.


## I INTRODUCTION

High-frequency groundwave radar measurements have demonstrated the feasibility of determining the fully developed ocean wave spectrum from sea backscatter. The range of groundwave radar measurements is limited to less than 200 km. Eventual application of HF measurements will be at skywave radar ranges extending out to 3000 km.

The second-order contributions to the Doppler spectrum obtained from HF sea backscatter measurements were modeled theoretically by Barrick [1] and Johnstone [2]. Assuming three forms of the fully developed ocean wave spectrum suggested by Phillips [3], Pierson and Moscowitz [4], and Tyler et al. [5], Johnstone found fair agreement between the theoretical

Doppler spectra and the observed Doppler spectra obtained from the ground wave radar experiments conducted at Wake Island by Tyler et al. [5]. The best agreement was found for the Pierson-Moscowitz form of the wave spectrum.

It is essential that an ocean wave spectrum can be determined uniquely from the backscatter data without assuming the sea is fully developed. A trial-and-error solution was employed to match the theoretical Doppler spectrum, based on an assumed ocean wave spectrum, to the observed Doppler spectrum. The purpose of this paper is to demonstrate the potential of using an HF skywave radar to remotely measure the ocean wave spectrum at distances up to 3000 km.

## II THEORY

The theoretical model of second-order HF radio-wave scattering from the sea derived by Johnstone [2] to determine the incremental surface radar cross section per unit area is used to estimate the ocean wave spectrum from HF skywave backscatter measurements. The radar cross section per unit area, $\sigma$, is

$$\sigma = \frac{4\pi R^2}{A} \frac{\left|E_S^R\right|^2}{\left|E_i^o\right|^2} \tag{1}$$

where A is the surface area of illumination, R is the distance of the transmitter and receiver from the target, $E_S^R$ is the scattered electric field measured at R, and $E_i^o$ is the electric field incident at the ocean patch. The effect of the scattering surface on the received power is expressed by the radar cross section. The radar cross section per unit

area per unit frequency for bistatic radar and vertical polarization expanded to first, second, and higher order is

$$\sigma_{vv}(\omega) = \sigma_{vv}^{(1)}(\omega) + \sigma_{vv}^{(2)}(\omega) + \text{higher order terms} \qquad (2)$$

where $\omega$ is the radian radio-wave frequency. The derivation of the expressions for Eq. (2) is found in Johnstone [2]. Proportional expressions that show the relationship of the ocean wave spectrum to the radar cross section per unit area per unit frequency are given. $\sigma_{vv}^{(1)}(\omega)$, the first-order term or Bragg line response, represents a resonant interaction of the ocean waves of length L equal to one-half the radio waves of length $\lambda$ and is proportional to the ocean wave spectrum, $W(\bar{k})$.

$$\sigma_{vv}^{(1)}(\omega) \propto W\left(\frac{4\pi}{L}, \quad 0\right) \delta(\eta \pm \omega_B) \qquad (3)$$

where $\delta(\eta \pm \omega_B)$ is the Dirac delta function, $\eta$ is the scatter radio-wave Doppler shift, and $\omega_B$ is the ocean-wave radian frequency for which first-order Bragg scattering occurs. Grazing incidence and monostatic geometry are assumed for the radar.

The amplitude of the Bragg lines in the theoretical Doppler spectrum calculated from Eq. (3) is not comparable to the amplitude of the Bragg lines in the observed Doppler spectrum because the former is power while the latter is power spectral density. $\sigma_{vv}^{(2)}(\omega)$ is the second-order term which results in the Doppler continuum and is directly comparable to the observed Doppler spectrum. Therefore, only the second-order contributions to the Doppler spectrum are compared. $\sigma_{vv}^{(2)}(\omega)$ is related to the ocean wave spectrum

$$\sigma_{vv}^{(2)}(\omega) \propto \frac{1}{L^4} \iint_0^{\infty\infty} \left(\Gamma_{EM}^2 + 4\Gamma_H^2\right) \delta(\eta \pm W_1 + W_2)\, W(\bar{k}_1)\, W(\bar{k}_2)\, dk_1\, dk_2 \qquad (4)$$

where $\Gamma_{EM}$ and $\Gamma_{H}$ are the electromagnetic and hydrodynamic kernels, respectively, and k is the radian ocean wave number.

## III THEORETICAL MODEL OF HF SECOND-ORDER SCATTERING FROM THE OCEAN SURFACE

The second-order radio-wave scattering model described by Johnstone [2] assumes a fully developed form of the ocean wave spectrum. Since the sea may be growing or decaying at the time of the backscatter measurements, the form of the ocean wave spectrum is unknown. Practical application of this model requires that for a given measured Doppler spectrum, a unique wave spectrum can be calculated. The required mathematical solution for this inversion operation has not been developed, however, and a trial-and-error solution is postulated. First, a form of the ocean wave spectrum is assumed. Second, a theoretical Doppler spectrum is calculated based on this ocean wave spectrum. Third, the theoretical Doppler spectrum in Eq. (4) is compared to the radar-measured Doppler spectrum. If the agreement is good, then the iterative solution is terminated. If not, adjustments are made in the assumed ocean wave spectrum and another iteration is performed.

The trial-and-error solution progressed in three steps. First, the fully developed form of the ocean wave spectrum suggested by Pierson and Moscowitz [4] was used:

$$W(\omega) = \frac{0.78}{\omega^5} e^{-0.74\left(\frac{g}{u}/\omega\right)^4} \tag{5}$$

where u is the wind speed and g is the acceleration due to gravity. The theoretical Doppler spectra obtained using Eq. (5) to describe the surface roughness were compared to the observed Doppler spectra. Second, if

satisfactory agreement was not found, then the shape of the ocean wave spectrum was changed for an assumed constant value of the amplitude and frequency of the spectral peak. This was accomplished by normalizing Eq. (5) to obtain

$$W(\omega \pm \omega_o) = \frac{A}{\omega^{N1}} e^{-B/\omega^{N2}} \frac{|S_p|}{|W_p|} \tag{6}$$

where A, B, N1, and N2 are constants that can be varied to change the shape of the spectrum, $|W_p|$ is the peak amplitude of the wave spectrum in Eq. (5), $|S_p|$ is the assumed amplitude of the spectral peak of the wave spectrum, and $\omega_o$ is a shift in the ocean wave frequency from the peak frequency in Eq. (5). A directional distribution for ocean gravity waves of $\cos^2(\theta/2)$ was assumed.

The theoretical Doppler spectrum is compared to the observed Doppler spectrum by matching the Bragg-line frequencies, $\Delta f$, and the peak amplitudes of the second-order contribution at $2^{1/2}\ \Delta f_1$ and $2^{3/4}\ \Delta f_1$. This is necessary, since the amplitudes of both the theoretical and observed Doppler spectra are in relative units. The fit was judged visually, according to the criteria described below.

The significant wave height, $\bar{H}_{1/3}$, was estimated from Eq. (5) or Eq. (6) by

$$H_{1/3} \cong 4\sigma \cong \int_0^\infty W(\omega)\, d\omega \tag{7}$$

where $\sigma$ is the standard deviation of the wave record based on a Rayleigh distribution function [6].

## IV SKYWAVE SEA BACKSCATTER MEASUREMENTS

High-frequency sea backscatter measurements relatively free of ionospheric perturbations were taken by WARF, a skywave radar located in central California on 12 February 1975 as part of the NORPAX experiment and other experiments. The data were obtained from a spatial average of the ocean waves in a 900-km$^2$ area located in the North Pacific Ocean at 29°N, 137°W. The radio-wave propagation was via a stable sporadic-E layer over the 1600-km distance from the radar to the illuminated ocean patch.

The sea backscatter data were analyzed by a range/Doppler processing technique. Four individual range resolution cells were processed for 102.4 s of integration to obtain a Doppler spectrum for each radar dwell. Two such Doppler spectra were incoherently averaged to obtain the reduced data shown in Fig. 1. In general, the skywave data are excellent, with minimal ionospheric perturbations.

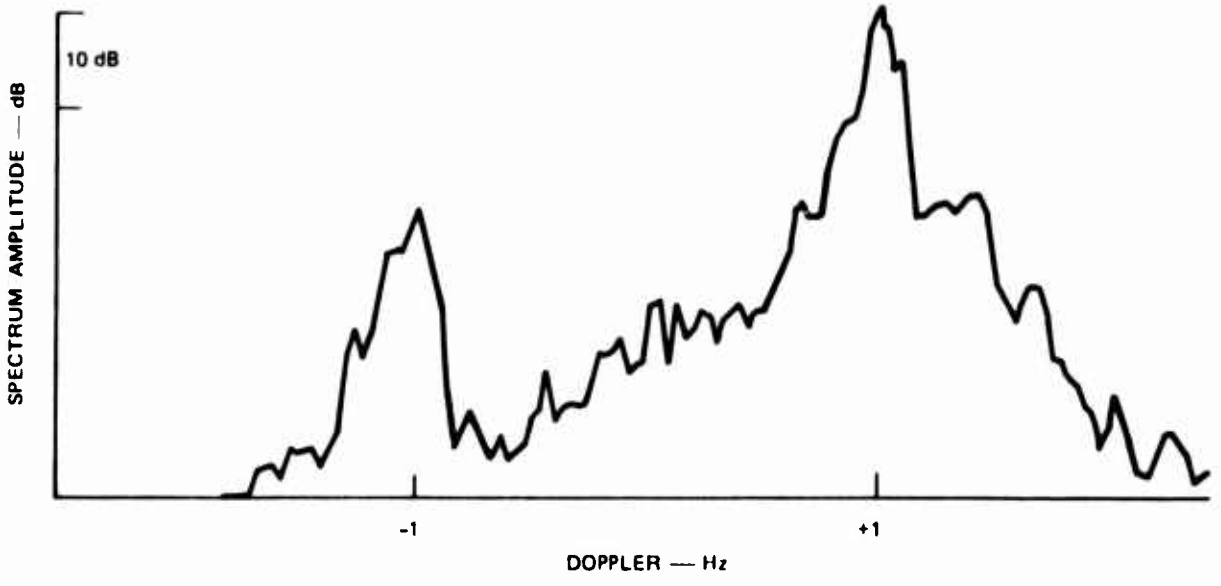


FIGURE 1 EXAMPLE OF THE OBSERVED HF SEA BACKSCATTER MEASUREMENTS TAKEN IN THE NORTH PACIFIC OCEAN

## V OCEAN WAVE OBSERVATIONS

Ocean wave spectra were not available for this experiment. Visual wave-height observations of 2.1 m and 1.5 m were obtained from two Navy ships operating in the experimental area. The empirical wave-hindcasting curves developed by Bretschneider [6] were used to predict the significant wave height. Two estimates of the surface wind were used--corrected surface geostrophic wind, and hourly wind reports obtained from the two Navy ships. The results are shown in Table 1. The estimates by all methods are within 10 percent.

Table 1

OBSERVED AND HINDCAST OCEAN WAVE HEIGHT

| Method | Corrected Surface Geostrophic Wind (m/s) | Mean Observed Wind (m/s) | Significant Wave Height (m) | Observed Wave Height (m) |
|---|---|---|---|---|
| CERC (1973) | 9.0 | 10.3 | 1.8<br>1.9 | |
| Visual Observation | | | | 1.8 |

## VI RESULTS

Comparisons of the second-order theoretical contributions to the Doppler spectra and observed Doppler spectra were made using the assumed ocean wave spectra given in Table 2 and shown in Fig. 2. These comparisons are shown in Fig. 3. The best fit between the theoretical and experimental

Table 2

OCEAN WAVE SPECTRA USED IN THE TRIAL-AND-ERROR SOLUTION

| Fig. No. | A | B | N1 | N2 | $S_P$ ($m^2 \cdot s$) | $W_P$ ($m^2 \cdot s$) | $\omega_o$ $\left(\frac{rad}{s}\right)$ | E ($m^2$) | $\bar{H}_{1/3}$ (m) | Direction Relative to Radar (degrees) |
|---|---|---|---|---|---|---|---|---|---|---|
| 2(a) | 0.78 | 0.351 | 5 | 4 | 1.080 | 1.000 | 0.000 | 0.556 | 3.0 | 170 |
| 2(b) | 0.78 | 0.740 | 5 | 4 | 0.430 | 1.000 | 0.000 | 0.264 | 2.1 | 170 |
| 2(c) | 0.78 | 1.500 | 5 | 4 | 0.177 | 1.000 | 0.000 | 0.130 | 1.4 | 170 |
| 2(d) | 0.78 | 2.225 | 5 | 4 | 0.108 | 1.000 | 0.000 | 0.088 | 1.2 | 170 |
| 2(e) | 0.78 | 0.100 | 5 | 4 | 5.075 | 1.080 | -0.251 | 0.415 | 2.6 | 170 |
| 2(f) | 0.78 | 2.225 | 5 | 4 | 0.108 | 1.080 | +0.377 | 0.875 | 3.7 | 170 |
| 2(g) | 0.78 | 0.740 | 5 | 4 | 0.430 | 1.000 | 0.000 | 0.264 | 2.1 | 160 |
| 2(h) | 0.78 | 0.740 | 5 | 4 | 0.430 | 1.000 | -0.251 | 0.264 | 2.1 | 160 |
| 2(i) | 0.78 | 0.740 | 5 | 4 | 0.430 | 1.000 | +0.251 | 0.264 | 2.1 | 160 |

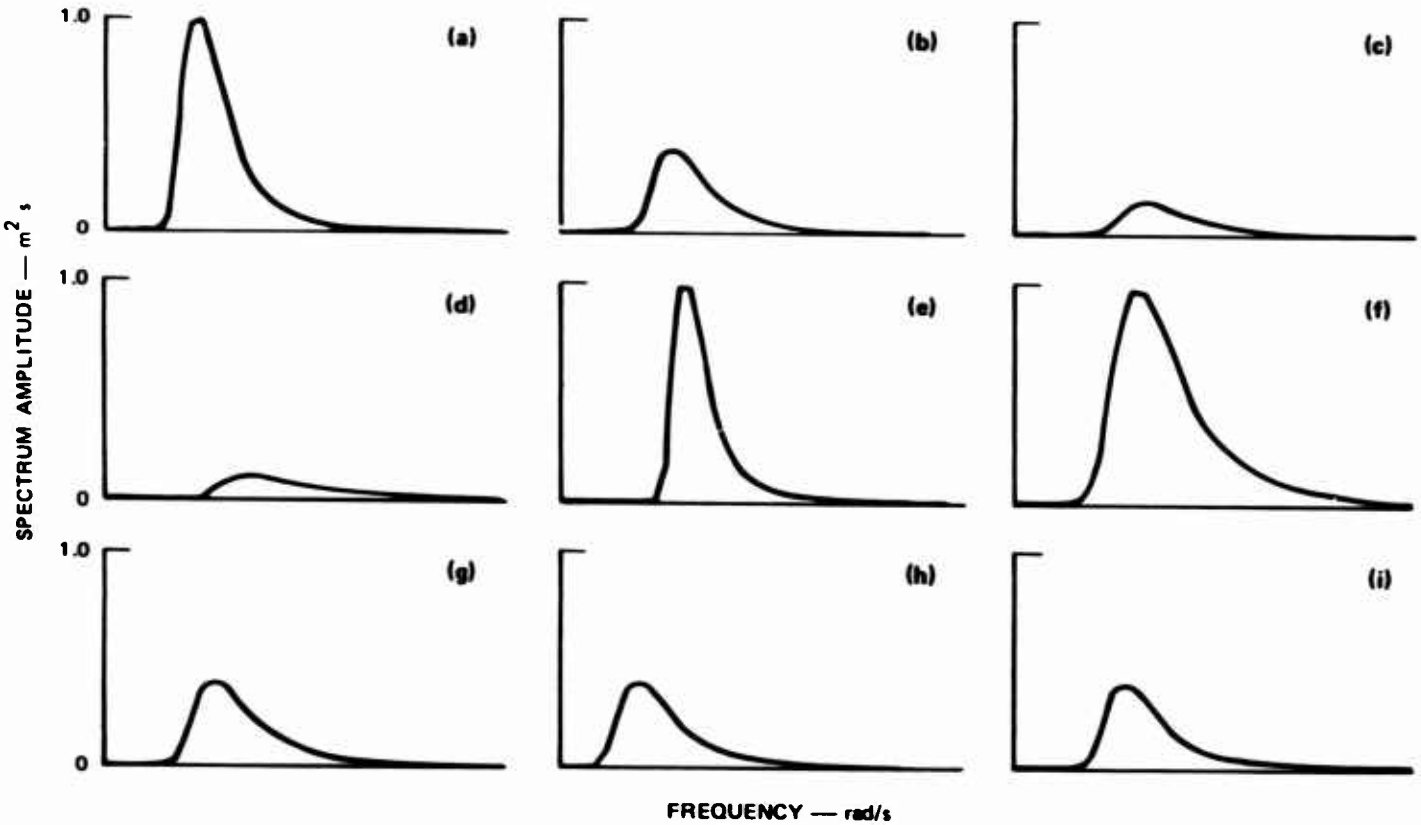


FIGURE 2 EXAMPLES OF THE OCEAN WAVE SPECTRUM USED TO DERIVE THE THEORETICAL DOPPLER SPECTRA

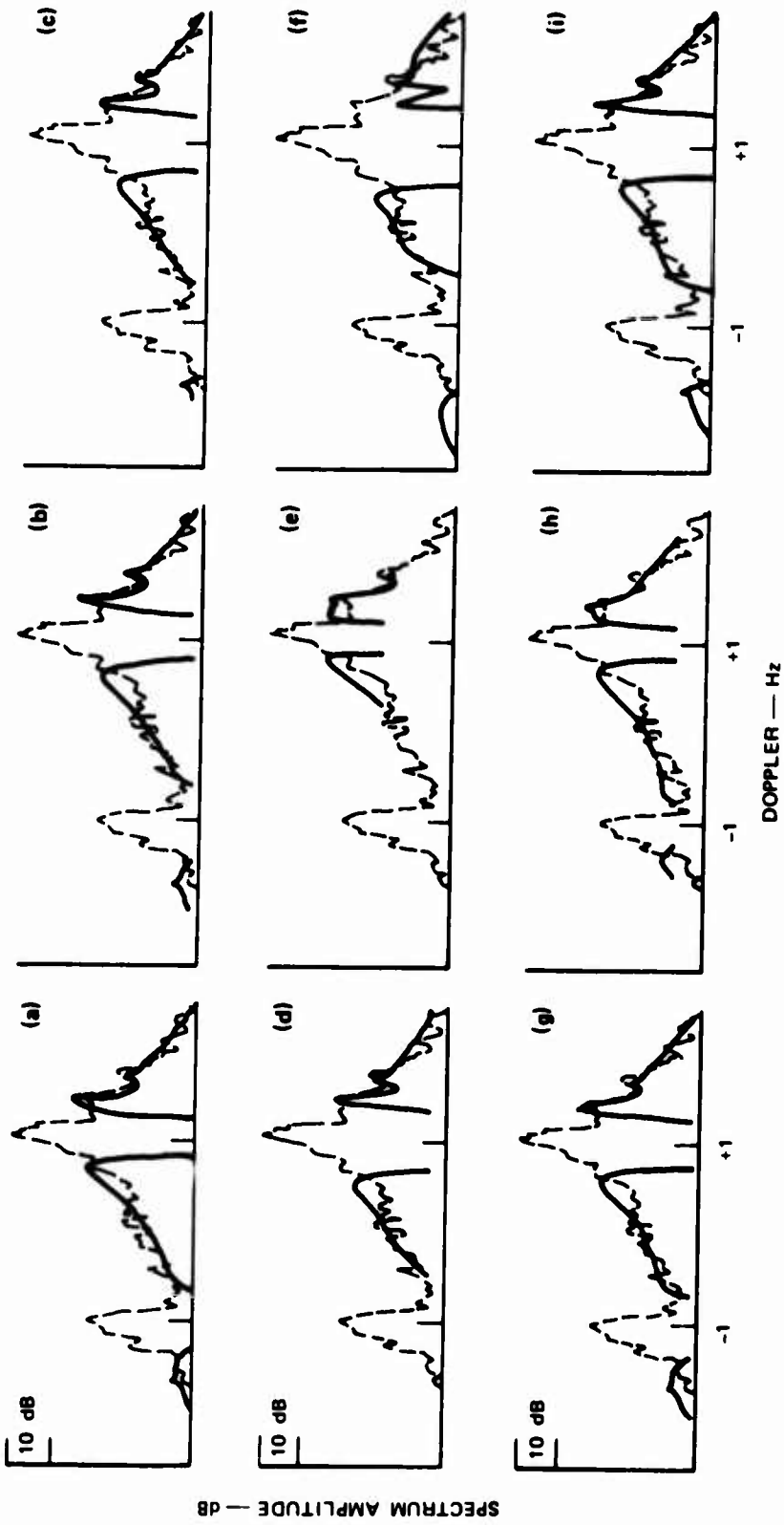


FIGURE 3 COMPARISON OF THE THEORETICAL AND OBSERVED DOPPLER SPECTRA FROM TABLE 1. The theoretical Doppler spectra are shown by the solid line and the observed Doppler spectra are shown by the dashed line.

Doppler spectra occurred for the ocean wave spectrum shown in Fig. 3(g) for waves approaching the radar at 160° from the radar bearing for

$$S(\omega \pm \omega_o) = \frac{0.78}{\omega^s} e^{-\frac{0.74}{\omega^4}} \qquad (7)$$

where $\omega_o = 0.000$. The visual fit was based on the match among the theoretical and observed cutoff values, slope of the Doppler continuum, and power from $2^{3/4}\ \Delta f_1$ to $\Delta f_1$. Since the comparison between the theoretical and observed Doppler spectra is made in dB, the maxima of the spectral fluctuations should be weighted more than the minima.

The comparison of the theoretical and experimental Doppler spectra is relative to the spectral peak at $2^{3/4}\ \Delta f$. The amplitude of the observed peaks at $2^{1/2}\ \Delta f_1$ and $2^{3/4}\ \Delta f_1$ may range ±2 dB, and the amplitude of the theoretical peaks are subject to calculation errors since they occur as discontinuities in the mathematical solution. Therefore, the fit of the entire second-order Doppler continuum was weighted more heavily in determining the best fit. The theoretical Doppler continuum outside the lower Bragg lines is slightly lower than predicted. A significant wave height of 1.9 m was calculated for the ocean wave spectrum given by Eq. (7), and is within 10 percent of the observed and hindcast wave heights.

The uniqueness of Eq. (7) is unknown. It can be argued from the trial-and-error calculation that other ocean wave spectra approximately equal in total energy can be derived using this technique. We attribute the close fit of several of the theoretical Doppler spectra to the observed Doppler spectra to the spectral fluctuations in the observed data.

For example, the fit between the theoretical Doppler spectrum derived from the ocean wave spectrum labeled Fig. 2(a) in Table 2 and the observed Doppler spectrum is also good. We did not choose this fit since the second-order contributions near the higher Bragg line appeared too high. On the other hand we can easily eliminate the fit for ocean wave spectra of more energy than Fig. 2(a) [Fig. 3(f)] and less energy than Fig. 2(a) [Fig. 3(d)].

The theoretical Doppler spectrum is particularly sensitive to the wave energy at each frequency as well as the total energy. The first four theoretical Doppler spectra shown in Figs. 3(a) through 3(d) were generated by an assumed form of the ocean wave spectra suggested by Pierson and Moscowitz [4] for mean wind speeds of 7.8 m/s, 8.7 m/s, 9.8 m/s, and 11.8 m/s. The theoretical Doppler spectra were influenced by the increased wave energy at the lower frequencies. The next two theoretical Doppler spectra shown in Figs. 3(e) and (f) were generated by a narrow peaked ocean wave spectrum and a broad ocean wave spectrum, respectively, at the same peak amplitude and frequency equal to the Pierson and Moscowitz form of the ocean wave spectrum for an 11.8-m/s mean wind. The differences in the resulting Doppler spectra are due to the difference in total wave energy at the various wave frequencies. It is interesting to consider idential ocean wave spectra at three different peak wave frequencies [Figs. 2(g), (h), and (i)]. An ocean wave spectrum shifted to lower frequencies results in a lower cutoff value and decreased energy in the Doppler continuum including the peaks at $2^{1/2}\ \Delta f_1$ and $2^{3/4}\ \Delta f_1$. An ocean wave spectrum shifted to the higher frequencies results in a higher cutoff value and increased energy in the Doppler continuum including the peaks at $2^{1/2}\ \Delta f_1$ and $s^{3/4}\ \Delta f_1$. The slope and energy content of the theoretical Doppler spectra change with contributions to the ocean wave spectrum at different frequencies. For a given shape of the ocean wave spectrum in which the total wave

energy may change, the theoretical Doppler spectrum increases in power but does not change slope.

## VII CONCLUSIONS

Long dwells necessary to obtain sufficient resolution in the Doppler spectrum can be obtained by skywave measurements. We have demonstrated a trial-and-error solution method to estimate the ocean wave spectrum. A comparison between the significant wave-height calculated from the ocean wave spectrum and the observed and hindcast significant wave heights showed agreement to within ten percent. Future work at determining the sensitivity of the measurement, the effects of swell generated from several distant storms, and the effects of the directional properties of ocean waves is warranted.

## REFERENCES


1. D. C. Barrick, "Remote Sensing of Sea State by Radar," Chapter 12, Remote Sensing of the Troposphere, V. E. Derr, ed., U.S. Government Printing Office, Washington, D.C. (1972).

2. D. L. Johnstone, "Second-Order Electromagnetic and Hydrodynamic Effects in High-Frequency Radio-Wave Scattering From the Sea," Technical Report No. 3615-3 (SEL-75-004), Stanford Electronics Laboratories, Stanford, Calif. (March 1975).

3. O. M. Phillips, "The Equilibrium Range in the Spectrum of Wind-Generated Ocean Waves," J. Marine Research, Vol. 16, pp. 231-245 (1958).

4. W. J. Pierson, Jr. and L. Moscowitz, "A Proposed Spectral Form for Fully Developed Wind Seas Based on the Similarity Theory of S. A. Kitaigordskii," J. Geophys. Res., Vol. 69, No. 24, pp. 5181-5190 (1964).

5. G. L. Tyler, C. C. Teague, R. H. Stewart, A. M. Peterson, W. H. Munk, and J. W. Joy, "Wave Directional Spectra From Synthetic Aperture Observations of Radio Scatter," Deep-Sea Research, Vol. 21, pp. 989-1016 (1974).

6. Shore Protection Manual, U.S. Coastal Engineering Research Center, Department of the Army, Corps of Engineers, Vol. I, Chapter 3, p. 157 (1973).